T.R.
BOLU ABANT İZZET BAYSAL UNIVERSITY
INSTITUTE OF GRADUATE STUDIES
Department of Physics

FEASIBILITY STUDY OF $Z_c(3900)$ EXOTIC STATE FOR PANDA EXPERIMENT

MASTER OF SCIENCE

SEDA YERLİKAYA

ACADEMIC SUPERVISOR
Prof. Dr. HALUK DENİZLİ

BOLU, AĞUSTOS - 2022

APPROVAL OF THE THESIS

FEASIBILITY STUDY OF Z_c (3900) EXOTIC STATE FOR PANDA EXPERIMENT submitted by SEDA YERLİKAYA and defended before the Examining Committe Members listed below in partial fulfillment of the requirements for the degree of **Master of Science** in **Department of Physics, Institute of Graduate Studies of Bolu Abant Izzet Baysal University in 02/08/2022** by

Examining Committee Members	**Signature**
Supervisor Prof. Dr. Haluk DENİZLİ Bolu Abant İzzet Baysal University	....
Member Assoc. Prof. Dr. Nuray ER Bolu Abant İzzet Baysal University	....
Member Prof. Dr. İlkay TÜRK ÇAKIR Giresun University	....

Prof. Dr. İbrahim KÜRTÜL
Director of Instıtute of Graduate Studies

ETHICAL DECLARATION

In this thesis dissertation that was properly prepared according to the Thesis Writing Rules of Bolu Abant İzzet Baysal University of the Institute of Graduates Studies, I hereby declare that;

- All data, information, and documents presented in the thesis were obtained in accordance with the academic and ethical rules,
- All data, documents, assessments, and results were presented in accordance with the scientific ethical and moral rules,
- All works that were benefitted in the thesis were appropriately cited,
- No alteration was made in the data used,
- Study presented in this thesis is original,

Otherwise, I declare that I accept the loss of all my rights in case any contradiction that may arise against me.

Based on the plagiarism report that was generated on the date of 02/08/2022 by using predetermined filtrations set by Directorate of Institute of Graduate Studies of the Turnitin programme, a plagiarism detection sofware, the similarity index detected was 11 %.

Seda YERLİKAYA

ABSTRACT

FEASIBILITY STUDY OF Z_c(3900) EXOTIC STATE FOR PANDA EXPERIMENT
MSC THESIS
SEDA YERLİKAYA
BOLU ABANT IZZET BAYSAL UNIVERSITY
INSTITUTE OF GRADUATE STUDIES
DEPARTMENT OF PHYSICS
(SUPERVISOR: PROF. DR. HALUK DENİZLİ)
BOLU, AUGUST 2022
(xvi + 84)

PANDA experiment, which is one of the physics programs of the FAIR Facility in the GSI physics center in Darmstadt, Germany aims to be one of the most important experiments in the hadron physics. The PANDA experiment, unlike other experiment (LHCb, Belle, BESIII and others) aims to investigate hadronic properties in different physical conditions and different environments. Particularly, the nature of the particles discovered by many researchers in recent years and the properties of exotic XYZ particles will be determined by the PANDA experiment. During the thesis study, the feasibility Z_c(3900) particle was carried out within the framework of the PANDA experiment. The analyzed Z_c(3900) particle contributed greatly to the expansion of the future physics program.

KEYWORDS: Particle physics, Egzotic states, PandaRoot software, PANDA dedector, PANDA physics program.

ÖZET

PANDA DENEYİ İÇİN Z_c(3900) EGZOTİK DURUMUNUN FİZİBİLİTE ÇALIŞMASI
YÜKSEK LİSANS TEZİ
SEDA YERLİKAYA
BOLU ABANT İZZET BAYSAL ÜNİVERSİTESİ
LİSANSÜSTÜ EĞİTİM ENSTİTÜSÜ
FİZİK ANABİLİM DALI
(TEZ DANIŞMANI: PROF. DR. HALUK DENİZLİ)
BOLU, AĞUSTOS - 2022
(xvi + 84)

Almanya'nın Darmstadt şehrinde GSI fizik merkezindeki FAIR tesisinin fizik programlarından biri olan PANDA deneyi hadron fiziğinin en önemli deneylerinden biri olmayı hedefliyor. PANDA deneyi, diğer deneylerden (LHCb, Belle, BESIII ve diğerleri) farklı olarak, farklı fiziksel koşullarda ve farklı ortamlarda hadronik özellikleri araştırmayı amaçlamaktadır. Özellikle, son yıllarda birçok araştırmacı tarafından keşfedilen parçacıkların doğası ve egzotik XYZ parçacıklarının özellikleri PANDA deneyi ile kesinleştirilecektir. Tez çalışması boyunca Z_c(3900) parçacığının PANDA deneyi çerçevesinde fizibilite çalışması yapılmıştır. Analizi yapılan Z_c (3900) parçacığının gelecek fizik programının genişlemesine katkısı oldukça fazladır.

ANAHTAR KELİMELER: Parçacık fiziği, Egzotik parçacıklar, PandaRoot yazılımı, PANDA Dedektör, PANDA fizik programı.

TABLE OF CONTENTS

LIST OF FIGURES

Page

LIST OF TABLES

Page

LIST OF ABBREVIATIONS AND SYMBOLS

APPA : Atomic Physics, Plasma and Applications
ASCII : American Standard Code for Information Intercharge
Barrel TOF : Barrel Time-of-Flight
BESII : Beijing Electron Pozitron Collider III
CAD : Computer Aided Design
CBM : Compressied Baryonic Matter
CLEO : Cornell Electron Storage Ring
CMS : Center of Mass System
CR : Collector Ring
EMC : Electromagnetic Calorimetry
FAIR : Antiproton and Ion Research Facility
FToF : Forward Time of Flight
FS : Forward Spectrometer
FT : Forward Tracking
FTS : Forward Tracking System
GEM : Gas Electron Multiplier
GSI : Helmholtzentrum für Schwerionenforschung GmbH
HESR : High Energy Storage Ring
JLAB : The GlueX experiment at the Thomas Jefferson National Accelerator
LHCb : The Large Hadron Collider Beauty
LMD : Luminance Monitor Detector
MDT : Mini Drift Tubes
MVD : Micro Vertex Dedector
MVS : Modularized Starter Edition
NUSTAR : Nuclear Structure, Astrophysics and Reaction
OBE : Signal-boson-exchange model
OPE : Signal-pion-echange model
PANDA : AntiProton ANnihilation at Darmstadt
PDG : Particle Data Group
PHSP : Phase Space
PID : Particle Identification

PMT : Plate PhotoMultiplier Tubes

RESR : Accumulارator Ring

RS : Muon Range System

SIMPs : Silicon Photomultiplier

STT : Straw Tube Tracker

TS : Target Spectrometer

UrQMD : Quantum Relativistic Quantum Molecular Dynamics

VLL : Vector Like Lepton

VMC : Virtual Monte Carlo

ACKNOWLEDGEMENTS

I am happy and proud to write these lines. Although I went through difficult processes, it is very nice to be happy to reach my dream.

First of all, I would like to thank my supervisor Prof. Dr. Haluk Denizli for including me in the project, providing my consultancy and giving me new experiences. This is my first project and it means a lot to me.

I would like to thank my study group friend Umut Keskin, who helped me during the study and the answered all my questions for everything.

Also, thank you very much to Prof. Dr. İzzet Morkan who always support me throughout my life.

Also, I am very happy to be a member of the PANDA Collaboration group.

I would like to thank the Scientific and Technical Research Council of Turkey (TUBITAK) for it is support to this thesis work within the scope of Grant No: 119F094

To my family

1. INTRODUCTION

In physics, only four fundamental forces are known in nature. According to the decreasing strength, they are strong force, electromagnetic force, weak force and gravitational force. Each of these forces has a physical theory. The strong force emerged in 1934 as a result of the work of Yukawa. It is mediated by the gluon. Strong theory is also called chromodynamics. The theory that explains the electromagnetic force is called electrodynamics. The classical formulation was given by Maxwell more than a hundred a years ago. Maxwell's theory was associated with special relativity. The quantum theory of electrodynamics was proposed by Tomonaga, Feynman and Schwinger in 1940. The electromagnetic force is mediated by a photon. The force that explains nuclear beta decay is called weak forces. The first theory about weak forces was put forward by Fermi in 1933. W and Z are intermediate vector bosons that mediate the weak force. The weak force theory is also called flavordynamics. The classical theory of gravity is Newton's law of universal gravitation. Relative generalization is Einsten's general theory of relativity. Gravitational has little effect compared to other forces in particle physics. It is mediated by graviton. Gravitational theory is also called geometrodynamics [1].

The Standard Model has twelve fermions and five bosons. Fermion is a subatomic particle with a single half-integer (1/2, 3/2….). It is divided into two groups: Quarks and Leptons. Quark is an elementary particle and one of the fundamental components of matter. The Eightfold Way was established in 1964 when Gell-Mann and Zweig independently proposed that all hadrons are composed of fundamental components that Gell-Mann called quarks. A quark's antiparticle is called an antiquark. Quarks are composed of up (u), down (d), strange (s), charm (c), bottom (b), top (t). Antiquarks are composed of antiup ($\bar{u}$), antidown ($\bar{d}$), anticharm ($\bar{c}$), antibottom ($\bar{b}$), antitop ($\bar{t}$). Each quark and each antiquark consists of three colors. Quarks are made up of the colors red, green and blue. So, there are a total of 36 quarks. The electric charge of the up, down, strange, charm, top and bottom quark is +2/3, -1/3, -1/3, 2/3, 2/3, -1/3, respectively. The electric charge of antiquarks the antiup, antidown, antistrange, anticharm, antitop and antibottom quark is -2/3, +1/3, +1/3, -2/3, -2/3, +1/3 respectively. Quarks consist of three generations. Up quark and down quark are first generation. Strange quark and charm quark are second generation. Bottom quark and top quark are third generation [1].

A lepton is a subatomic particle that responds to electromagnetic force, weak force, gravitational force but not to strong force. Lepton is the fundamental particle and building block of matter. Leptons are composed of electron (e^-), electron neutrino (ν_e), muon (μ^-), muon neutrino (ν_μ), tau (τ^-) and tau neutrino (ν_τ). Antimatter particles are denoted by the symbols of (e^+), (μ^+), (τ^+) for the charged leptons and $\bar{\nu}_e$, $\bar{\nu}_\mu$, $\bar{\nu}_\tau$ for the neutral leptons. The first generation electron and electron neutrino are called electronic leptons. The second generation muon and muon neutrino are called muonic leptons. The third generation tau and tau neutrino are called tauonic leptons. The electric charges of electron, muon, tau are -1 while the electric charges of electron neutrino, muon neutrino, tau neutrino are 0 and leptons have a spin of ½ [1].

In 1933, an event that occurs at a single point and does not require an intermediary particle was discussed in the beta decay theory. The range of weak force is short due to beta decay. Thus, while the Fermi's model gives approximate results at low energies, this result may fail at high energies. It has been accepted to replace it with the theory that some particles are mediated and mediator is called the intermediate vector boson. In this theory, there are three intermediate vector bosons: two charged ($W^\pm$) and one neutral (Z). Boson is a subatomic particle whose spin quantum number has an integer value (0, 1, 2…). Bosons consist of gluon, photon, W&Z boson and Higgs boson. Gluons form photons and neutrons, creating the strong nuclear force that binds quarks together. The W&Z bosons belong to the weak nuclear force. Photons are quanta of light that transmit electromagnetic force. The observed subatomic particles are either a boson or fermion [1].

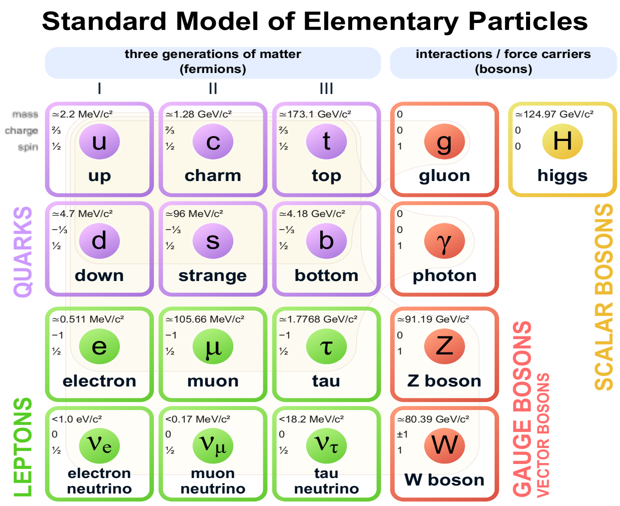

Figure 1.1. Standart Model of Elementary Particles [2].

1.1 Exotic Particles

Exotic particles are used to describe particles with different properties that do not resemble the properties of any particle in the Standard Model. Some particles discovered during the CLEO, Belle, DO, CDF, LHCb and BESS experiments are called “exotic particles” because of their non-standard structure. These different structures are XYZ particles, gluontops, hybrids ($q\bar{q}q$ or qqqq), meson moleculs ($qq\bar{q}\bar{q}$), tetraquarks (q $\bar{q}$ q $\bar{q}$), pentaquarks (qqqq $\bar{q}$), hexaquarks ($qqqqqq$ or $\bar{q}\bar{q}\bar{q}\bar{q}\bar{q}\bar{q}$). Many charmonium and botonium-like XYZ particles have been discovered. Recently discovered particles h_c, X_{c2}(2P), B_c^+, η_b(1S) have been also added to the list of exotic particles. These particles are not thought to belong to the Standard Quark Model. Most of these particles needs to be proven by experimental studies [3].

Examination of exotic particles are important in terms of the formation of the universe, dark matter, dark energy and the internal structure of neutron stars. Thanks to advances in experimental technology, exotic particles have become easier to detect after examining the signals and background signals of the sought particle. In the literature, structure of these exotic particles are discussed as : Tetraquark, Pentaquark, Hekzaquark, Hybrids, Molecule, Gluonballs [3].

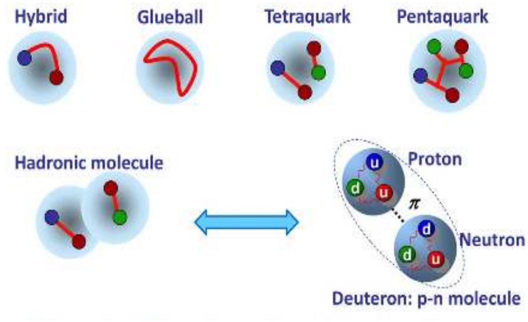

Figure 1.2. Exotic particle classes [4].

1.1.1 Tetraquarks

$[q\bar{q}][q\bar{q}]$, one of the way of forming an exotic particles is the combination of two quarks with a certain color quantum number and two antiquarks with two anti-color charges, Tetraquarks. They are formed by the decay of B meson and have a lifetime of approximately 10^{-24} seconds [3].

In 2003, the particle named X(3872) was thought to be a tetraquark by the Belle experiment in Japan. Scientists couldn't prove it because they didn't have enough evidence. In 2007, scientists thought that the Y(4660) particle might exist. In 2009, scientists announced that they had found a new particle Y(4140). This particle decayed into two mesons. Scientists thought that this particle might contain a charmed and anti-charm quark. In 2008, scientists discovered Z(4430) particle in the decay of B mesons with the Belle experiment. This particle has been proven by B meson decay as a result of proton-proton collision in the LHCb experiment in more than 25.000 data analyses. Later in 2010, it was thought that the Y(5S) meson might be a tetraquark. The $Z_c(3900)$ particle was discovered by two independent groups in 2013. When the $\psi(4260)$ particle decays, the Zc(3900) particle were observed and the $Z_c(3900)$ particle was thought to have four quarks. As a result, the existence of tetraquarks was confirmed by the LHCb in 2014. The structure of these particle was thought to be same as the structure of the atom. According to the observed results, the new particles with greater masses are X(4140), X(4274), X(4500) and X(4700) [3].

1.1.2 Pentaquarks

In the thinking of high energy physicists, the pentaquark is a subatomic particle made up of four quarks and one antiquark [3].

According to the results of the work done in the bubble chamber experiment at Moscow ITEP in 1986, a peak of 1.54 GeV was observed. In 1997, a group of scientists suggested the existence of pentaquarks, according to studies at the Petersburg Institute of Nuclear Physics. In 2002, researchers from Osaka University thought that bombarding a carbon target with X-rays might provide clues to the existence of pentaquarks. The discovery of pentaquarks was made at the Jefferson laboratory in the USA in 2003. Other evidence for pentaquarks are the observation of the $ssdd\bar{u}$ (electric charge is -2e and mass value is 1862 MeV) and $uudd\bar{c}$ (neutral and mass value is 3099 MeV). These particles were named $\phi(1860)$ and $\theta_c(3100)^0$, respectively. According to experiments at the LHCb in 2015, two unknown particles were been discovered about 4.7 times heavier than the proton mass and the other slightly heavier. When this work was analyzed, the particles contained one c, one $\bar{c}$, two u and one d quark. In 2015, pentaquarks $P_c^+(4380)$ and $P_c^+(4450)$ containing two charm quarks were discovered by the $\Lambda_b^0 \rightarrow J/\psi\ p\, K^-$ in collaboration with LHCb. Such particles could not be explained by the Standard Quark Model and the new versions. The single-boson-exchange model (OBE) and the single-pion-exchange model (OPE) are presented to explain the properties of these particles [3].

1.1.3 Molecular Structure

In the quark model, the four quark states are classified according to their internal structure as $[qq][\bar{q}\bar{q}]$ and $[q\bar{q}][q\bar{q}]$. The first of these two kinds of quarks are called $[qq][\bar{q}\bar{q}]$ tetraquark. These exotic particles have light quarks are called light tetraquarks. The second type consists of two light mesons interacting with each other. This particle is called a molecule [3].

Among numerous discovered charmonium-like states known as XYZ particles in the charmed hadron group (D and D_s mesons), B factories detected two particles with narrow decay widths: $D_{s0}^*(2317)^{\pm}$ and $D_{s1}(2460)^{\pm}$. Mass and width of these particles are small and narrow according to the calculations in the Standard Model and much smaller than the mass expected for $c\bar{s}$ mesons. So $D_{s0}^*(2317)^*$ and $D_{s1}(2460)^{\pm}$ quadruble may be considered as tetraquark states or $DK(DK^*)$ molecular states. The best candidates in the group of molecules were identified by the Belle experiment as X(3872) particle and X(4430) particle. In addition, $Z_b(10610)$ and $Z_b(10650)$ particles are also molecular structure candidates [3].

In 2017, new charmonium-like states were discovered by the BESIII experiment. The Y(4320) particle is observed in the $e^+e^- \to \pi^+\pi^- J/\psi$ process and Y(4390) particle is observed in the $e^+e^- \to \pi^+\pi^- h_c$ reaction. These particles are vector particles. Scientists have observed many vector particles with masses in the range of 4 to 4.6 GeV in their experiment. This region has the mass region for many exotic hadrons with a charm quark-antiquark. The investigation of these particles is important for molecular structures [3].

1.1.4 Hybrids Mesons

In the Standard quark model, mesons have the $q\bar{q}$ structure and characterized by $I(J^{PC})$ quantum numbers. I is isospin, J is total angular momentum, P is pariety, C is charge conjugate. The hybrids are expected to have masses of about 2 GeV and decay into two mesons. Quantum numbers 0^{-+}, 1^{-+}, 1^{--}, 2^{-+} mass values of hybrid particles should be in the range of 1.7-1.9 GeV. According to lattice theory, 1^{-+} have exotic quantum numbers hybrids mass is about 1.9±0.2 GeV. According to researchers $\pi_1(1370)$ low-mass exotic meson. This particle may be hybrid meson or tetraquark. Additionally, $\pi_1(1440)$, $\pi_1(1625)$ and $\pi_1(2000)$ particles may be hybrid [3].

1.1.5 Baryonium, Dibaryon and Hexaquarks

Baryonium, dibaryon and hexaquarks particles can form particles with structures different from six quarks. If the particle consists of six quarks, the baryon number is two and this particle is called a “dibaryon”. The d^*(2380) particle consisting of u and d quarks is a dibaryon. Baryonium states can be confused with meson and tetraquarks but dibaryons do not mix with hadrons since the baryon number is conversed. So, they are easy to identify. If the particle consist of the three quarks and three anti-quarks, this system is also called hexaquark. Hexaquarks like tetraquarks and pentaquarks can be in the form of multiple quarks or a baryon-baryon molecule. If the particle consist of the three quarks and three anti-quarks, the baryon number is equal to zero, and this state is called “baryonium”. $f_2(1565)$ particle considered to be a baryonium candidate [3].

1.1.6 Glueballs

Fritzch and Gell-Mann for the first time in 1972 thought that mesons made up of gluons might exist. In 1975, Fritzch and Minkowski said that glueball states are a new type of matter and the result of the quark-gluon field theory. In 1977, D. Robson stated that scaler mesons would consist of an ideal nonet mixture. Most of the η'(958) particle has been studied as glueball. Although 40 years have passed, no clear information on this subject has been reached. Physicists have been searching for hypothetical particles called glueballs, consisting only of gluons for nearly 40 years. Since these particles are unstable, they can be observed by analyzing their decay [3].

The most important process is J/ψ decay in glueballs production and the decay width of J/ψ is narrow. J/ψ decays into three gluons in most decays and turns into hadrons but J/ψ can also decay into two gluons and a photon. Photon can be detected. Thus, two gluons can interact to form glueballs. According to studies, glueballs can be produced in central collisions. In central collisions, two hadrons pass without touching each other. The valance quarks do not exchange, while the two hadrons are diffracted in the forward direction. This process is called Pomeron-Pomeron scattering [3].

In 2014, the GlueX experiment at the Thomos Jefferson National Accelerator (JLAB) was designed to detect gluballs. The purpose of this experiment is to map the spectrum of exotic mesons by excitation of the gluon field holding the quarks together and to understand the unexplained entrapment phenomenon of KRD.

Scientists believe that complete information about glueballs will be confirmed by the information obtained from Gluex, BESIII and PANDA experiments [3].

1.2 The Exotic Z_c(3900) Particle

The exotic Z_c(3900) particle was observed by BESIII and Belle Collaborations and this particle thought to be a hadron. Many events related to the Z_c(3900) particle emerged when the two collaborations conducted investigations together. The resonance structure of the Z_c(3900) particle has been experimentally tested by Y(4260)→ $J/\psi\pi\pi$ and Y(4260)→ $\overline{D}^{*}D\pi$. As a result of Z_c(3900) particle studies, it has been revealed that the $\psi(4260)$ particle is a decay product. Z_c(3900) particle decays into a charged pion ($\pi^{\pm}$) and a j/ψ meson. The mass of the Z_c(3900) particle is approximately 3900 MeV. This is associated with Z_c(3900) particle with four or more quarks. Discovery of neutral Z_c(3900) particle was learned by CLEO-c [5].

In this thesis, full simulation of $Z_c(3900)^{-}$ exotic particle with Panda Software is studied via $\psi(4260) \rightarrow Z_c(3900)^{-} + \pi^{+}$ decay channel where $Z_c(3900)^{-}$ decays to J/ψ and π^{-}. J/ψ particle is a subatomic particle composed of the charm quark and the charm antiquark. The mass of this particle is approximately 3.1 GeV/c^2 and the particle was discovered by two American physicists in 1974. One group made the discovery at physicist Burton Richerter's Standard Linear Accelerator Center and the other at physicist Samuel Ting's Brookhaven National Laboratory. Richter and Ting were awarded the 1976 Nobel Prize in physicis for this discovery. The discovery of the J/ψ mesons revealed the existence of the fourth quark, the charm quark. Leptonic decay of J/ψ is considered in this thesis, i.e. $e^{+}e^{-}$ or $\mu^{+}\mu^{-}$. The beam energy is set to produce $\psi(4260)$ particle in resonance. The particle $\psi(4260)$ is a particle with a mass of 4230 MeV that does not belong to traditional quark model and this particle was discovered by the BaBar experiment. The charmonium like $\psi(4260)$ particle state has been studied by the BABAR Collaboration on the process $e^{+}e^{-} \rightarrow \pi^{+}\pi^{-}j/\psi$. This work was approved by the CLEO Collaboration. The nature of $\psi(4260)$ particle some features are unusual for the charmonium. This is particles made up of

D mesons or a state of four quarks. The BaBar experiment has discovered situations that have not been observed since 2003. When the $\psi(4260)$ and $Z_c(3900)^-$ particles are discovered, researchers should pay attention to the complex structures of the particles. Therefore, final state particles in decay channel under consideration for the seach of $Z_c(3900)^-$ are e^+, e^- , π^+ and π^- or μ^+, μ^- , π^+ and π^- [6,7].

2. PANDA Experiment

The hadron physics program at the FAIR facility is examined in the PANDA experiment studies and it is located in the district of GSI Helmholtzentrum für Schwerionenforschung GmbH in Darmstadt. The PANDA experiment plans to make precise measurements by analyzing the end state particles produced due to the collision between the antiproton beam and different fixed target. Panda's goal is to try to understand properties of hadrons: masses and widths, etc.. The antiprotons produced by the primary proton beam will be filled into the high energy storage ring [10]. The PANDA Collaboration plans to explore a wide range of topics in the field of weak and strong forces, nuclear structure, exotic states of matter, atomic and plasma physics [8].

2.1 Accelerator Facility

FAIR, the International accelerator Facility for Antiproton and Ion Research in Europe, is built to achieve stable beams covering a wide range of intensities and beam energies. The accelerator facility will consists of magnets, cryo technology, rf technology, vacuum etc. relates to system. FAIR will use heavy ion synchrotrons, antiproton and isotope generation stations, high resolution separators, several storage rings where beam cooling can be applied. Intensive work on the test infrastructure for the superconducting magnet of FAIR machines are being done at GSI and other laboratories. The GSI accelerator facility serves as the injector for FAIR accelerators. FAIR research consists of four experimental steps: NUSTAR, CBM, PANDA, APPA [9].

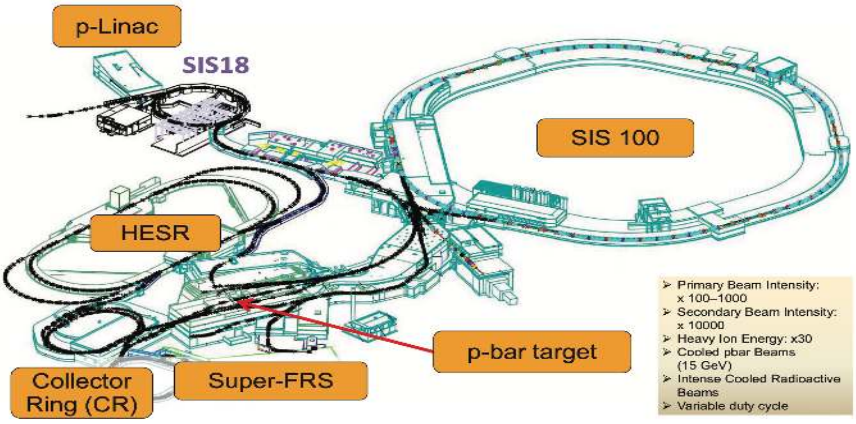

Figure 2.1. Shows the planned layout of the FAIR facility [9].

The FAIR facility will be constructed on approximately 150.000 m^2 adjacent to the GSI site. The FAIR accelerator feature of the Modularized Starter Edition (MSV) is shown in Figure 2.1 above. The FAIR accelerator plant is a synchrotron accelerator ring with a magnetic hardness of 100 Tm-SIS100. The circumference of the synchrotron is about 1100. It will be installed in a 20 m deep tunnel. In the next phase of the project, the installation of the SIS300 synchrotron is designed. For the highest intensities, the SIS100 should operate at a 1 Hz repetition rate. Therefore, it is planned to operate the dipoles at ramp speeds up to 4 T/s. The task of the collector ring (CR) is to provide stochastic cooling of radioactive ions or antiproton beams from production targets [9].

2.2 Scientific Program of FAIR

There are many scientific programs under consideration in FAIR facility. PANDA is one of them. Some of these scientific programs are briefly discussed in the following sub sections [9].

2.2.1 NUSTAR (Nuclear Structure, Astrophysics and Reaction)

The NUSTAR collaboration is divoted to nuclear structure, astrophysics and reaction study. FAIR-NUSTAR will be one of Europe's leading facilities. One of the future antiproton and ion research facility in Darmstadt is the NUSTAR facility.

NUSTAR collaboration includes both experimental and theoretical programs when the NUSTAR physics program provides the ideal interaction to answer challenging quaestions. The NUSTAR facility will enable the exploration of nuclei at the stage related to energy production and element synthesis. At the same time, the NUSTAR facility will cover electron scattering or antiproton-ion collisions on exotic nuclei [10].

2.2.2 CBM (Compressed Baryonic Matter)

The Compressed Baryonic Matter (CBM) detector will detect both proton-nucleus and nucleus-nucleus collisions at beam energies up to 45 GeV. In the CBM, electrons will be detected using a RICH dedector with a gas of silicon tracking stations placed within a magnetic dipole moment. The CBM experiment will calculate hadronic and leptonic probes with a large phase space [11].

2.2.3 PANDA (antiProton ANnihilation at DArmstadt)

The purpose of the PANDA experiment is to exploit the antiproton beam in the High Energy Storage (HESR) as a result of the collision of an internal proton target and spectrometer for a rich hadron physics program. PANDA experiment investigates Charmonium, Open charm spectroscopy and status of exotic hadrons [12].

2.2.4 APPA (Atomic Physics, Plasma and Applied)

APPA is a research experiment working on Atomic Physics, Plasma and Applied sciences. The APPA science program will use full parameter range of FAIR [13].

2.3 PANDA Physics Program

The PANDA experiment in Darmstadt, Germany provides a brief overview of the PANDA physics program. PANDA is a physics program that contains information about hadron structure, quark-gluon dynamics, nuclear physics in both $\bar{p}p$ and $\bar{p}$-nucleus collisions. Feasibility studies and feasibility comparisons can be found in the PANDA physics performance report. The PANDA research program at FAIR will explore important questions for understanding strong interactions [12].

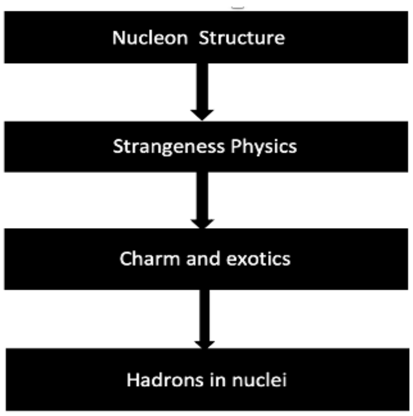

Figure 2.2. Panda Physics Program Diagram [14].

2.3.1 Nucleon Structure

Nucleons are formed from basic components called quarks by the charge of gluons. Subjects (such as hadron spectroscopy in the harmonium mass, the properties of hadrons in nuclear matter, hypernuclear physics or nucleon properties) using electromagnetic processess are part of PANDA's physics program. The main part of this contribution focuses on the feasibility of measuring using electromagnetic processes at PANDA. An antiproton with a beam momentum up to 15 GeV/c would be enabled in a nuclear physics program. After leptons beams became available, scientists began to study the structure of the nucleon. Elastic electron proton scattering has been studied to describe the electromagnetic properties of the proton. The electromagnetic process class distinguishes a universal non-perturbative hadronic element whose amplitudes include structure functions like perturbative parton distribution functions and generalized parton distributions [14].

2.3.2 Strangeness Physics

Strangeness is a particle property described as a quantum number when the particles decay in strong and electromagnetic interactions in a short time. The strangeness of a particle is the sum of the strangeness of the quarks formed [15].

In the early studies of high-energy physics, cosmic rays were the only reason for the emergence of high-energy particles. Researchers set up bubble chambers to observe particles coming from the atmosphere to the Earth's surface. These particles are electrons and protons. In the late 40s and early 50s, researchers noticed a new particles called "strange particles". When these particles decay, they take the v shape. These discovered particles are heavier than pion and proton [15].

2.3.3 Charm and Exotics

The quark model describes mesons and baryons. Mesons are known as quark–antiquark states interacting via a potential. Glueballs are formed due to the self–essembly of color charged gluons. This unique feature of the strong interaction is of interest because the sticky ball mass is not effected by the Higgs mechanism. Thus, it is generated dynamically by strong interaction. It is difficult to determine the cohesive sphere state of the observed hadronic state. Researches for exotic hadrons continue at different energy scales from the light u and d scale to the bottom quark scale. Different observations are expected for the physics of hidden charm states such as charmonium, due to the high mass of the charm quark. Meson – like systems composed of heavy and like quarks, such as open charm states, complement hidden charm meson - like states [14].

Mechanisms regarding the production mechanisms of open charm meson and baryon pairs in proton-proton collisions will be similar. Attractiveness is protected under strong electromagnetic interaction but not protected under weak interaction. Open-charm spectroscopy and electroweak process will be achievable in PANDA’s later stages. PANDA should have a peak and a good statistical calculation [14].

2.3.4 Hadrons in Nuclei

The first important theory of the strong force was established by Yukawa in 1934. Yukawa thought that the proton and neutron were attracted to each other by a kind of unknown field. Yukawa asked , what should be the properties of quantum, and which particle would take into account the known properties of the strong force. For example, the force’s short range indicates that the vehicle would be quite heavy. Yukawa has calculated the mass by considering it to be about 300 times as the mass of an electron or about one-sixth the mass of a proton. Yukawa’s particle was considered as a meson because it has a value between the electron and the proton. The electron was named a lepton (light weight), the proton and neutron were named a baryon (heavy weight). Yukawa assumed that his theory was wrong, thinking that these particles were not observed in the laboratory. At that time, two groups of researchers were conducting a series of systematic studies on cosmic rays. They have detected particles matching Yukawa’s description. When cosmic ray particles were studied in detail, it was shown that the particle mass was lighter than what Yukawa has predicted. In 1946, definitive experiments were carried out showing that cosmic ray particles interact weakly with atomic nuclei. In 1947, Powell has discovered pion and muon particles in cosmic rays. While searching for Yukawa’s meson, the muon had nothing to do with strong interactions. In fact, it behaves like a heavier version of the electron and belongs to the lepton family [1].

Baryons are more difficult to be analyzed than mesons. The baryon has three bodies. If each baryon consists of three quarks, each antibaryon consists of three antiquark. There is only one orbital angular momentum that needs to be considered. The baryon’s angular momentum consists of the combined spins of the three quarks. Three quarks probably have eight states (↓↓↓), (↑↑↓), (↑↓↑), (↑↓↓), (↓↑↑), (↓↑↓), (↓↓↑), (↓↓↓) because quarks have up spins and down spin. If a meson contains a red quark, it must also contain an antiquark. At the same time, each baryon must have a quark of each color [1].

2.4 PANDA Detector

The PANDA detector is under construction at the future FAIR facility in Darmstadt, Germany. A key component of the GSI facility is the High Energy Storage Ring for high-density, phase-space-cooled antiprotons with momentum up to 15 GeV/c. A physics program is planned at this facility to investigate the structure of hadrons in the charmonium mass range and the spectroscopy of double hypernuclei. In addition, a general purpose detector called PANDA (Proton ANTİProton Detector Array) has been constructed to serve many of the experiments planned at this facility. An overwiev of the PANDA detector concept will be presented and selected as a results of the simulation of detector performance will be discusssed. PANDA name stands for anti-**P**roton **AN**nihilations in **Da**rmstadt [16].

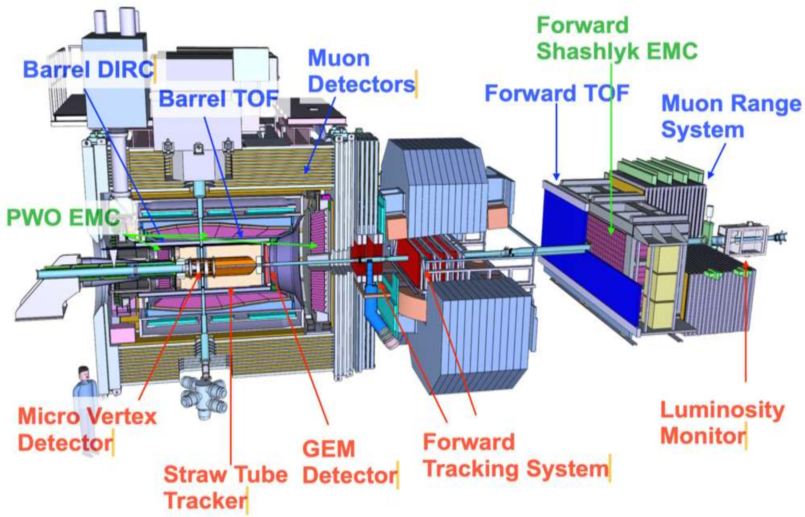

Figure 2.3. Top view of the PANDA apparatus [14].

The dedector shown in the Figure 2.3 was constructed from two spectrometers to obtain a good momentum resolution. Expected gains in spectrometer design are acceptance of close to 4π, high tracking resolution, particle identification (PID) and desired brighteness. The parts of the detector are described below [17].

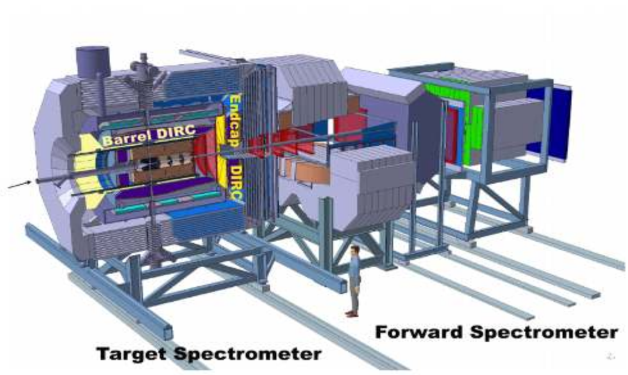

Figure 2.4. PANDA detector includes target and advanced magnetic spectrometer. This table shows the sub-dedector of the solenoid and the sub-dedector in behind the dipole magnet. DIRC dedectors in the target spectrometer are shown in light colors. The ray comes from where the arrow is pointing [18].

The two magnetic spectrometer configurations are shown in Figure 2.4. The part inside the conductive solenoid magnet surrounding the spectrometer interaction point is called the Target Spectrometer (TS). The solenoid in the interaction region and a dipole-based region are called a Forward Spectrometer (FS) that could be used for momentum analysis of forward particles. [19].

2.4.1 Barrel DIRC

PANDA Barrel DIRC is a part of the particle identification (PID) system for the PANDA detector to be installed at the Antiproton and Ion Research Facility (FAIR) in Germany. Barrel DIRC will define a hadronic charged particle in the angle range of 22^0 to 140^0 for particle momentum between 0.5 GeV/c and 3.5 GeV/c. Barrel DIRC uses a spherical lens as a narrow rods and anprism-shaped expansion as a volume system. The design of Barrel DIRC was developed using Monte-Carlo simulation [20].

Low momentum traces below the kaon threshold are considered kaons when detectors are operated in veto mode. Here, the purity of the kaon sample depends on the detailed composition of the background. Photons are recorded by photon detectors. The focusing lenses at the end of the radiator rods form an image in the plane of the photon detector. The performance of DIRC in term of photon yield should be examined within the framework of the PandaRoot simulation. In a fixed target experiment, most photons will hit the mirror because the angular distribution of the charged particles is advanced. Asimulation of an improved design is given in Figure 2.5 [20].

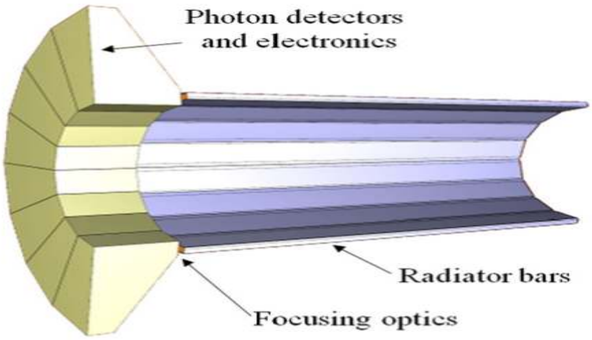

Figure 2.5. Upstream view of the PANDA Barrel DIRC. Photons propagate through radiator until they hit the back of the expansion box. Here, they are recorded by pixelated photodetectors [21].

The design consists of $2500\times17\times35\ mm^3$ radiator rods made of synthetic fused silica. There are two spaces for the vertical beam pipe on above and below the barrel. Pixel size of photon detectors is $6.5\times6.5\ mm^2$. The focusing lens creates a sharp image of Cherenkov photons between the radiator and the expansion volume. The pixel size adds 6.3 mrad to the single-photon Cherenkov angle resolution. Chromatic angular resolution benefits to 5 mrad. These values depend on the combined single photon resolution of 8-9 mrad [22].

2.4.2 Barrel TOF (Barrel Time-of-Flight)

The Barrel TOF dedector is a cylindrical detector approximately 50 cm radial from the beam and assists as a precision timing detector. This dedector is in high magnetic field, so non-magnetic materials had to be used. Studies will begin in 2025 with experiments on antiprotons. Selection is regulated by Barrel TOF's online software framework for calculating event sequencing. The event time of all particles is calculated from the momentum information of the monitoring system. For low momentum particles separation can be achieved, while for high momentum particles identification will be done by the Barrel DIRC detector [23].

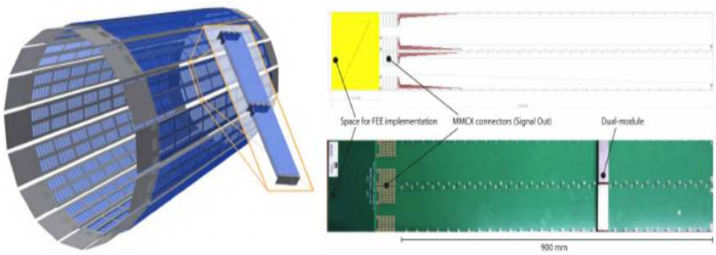

Figure 2.6. (Left) Structure drawing of the file with the help of double scintillator of the barrel TOF (Right) Supermodule circuit is above design [23].

The Barrel TOF consists of 16 independent section from 22.5^0 to 140^0 around the beam axis as shown in Figure 2.6. They can be conbined into a single channel to increase the sensitive area without increasing the number of read channels. There are different ways to connect Silicon Photomultiplier (SİMPs), serial, parallel or hybrid . Although the bias for parallel connection is common by all SİMP, the signal response is slow. In parallel connection the signal response is slow whereas in serial connection the signal response is fast [23].

Optimization studies were carried out in terms of the best time resolution material and geometry resulting in the design. Barrel TOF dedector identifies particles at low momentum. As a result of the study, an internal time resolution of $\sigma t = 54\, ps$ was obtained in the laboratory [23].

2.4.3 Muon Dedectors

Muon detector in PANDA is based on a range system made up of iron layers. It is sufficient to use the hadron calorimeter for the resolution of the Muon System. The Muon system consist of four parts: a Barrel (13 layers), an EndCap (5 layers), a Muon Filter (4 layers) and a Forward RS (16 layers) [24].

Good muon identification is required to measure muons over a wide momentum range the in PANDA experiment. The Drell-Yan process is a choice for optimizing the PANDA muon system. The muon is identified by different detector systems and methods. A very good muon identification is assumed to control the signal to background ratio. The first system is considered the main system for reliable muon identification but other systems can be considered important complements [25].

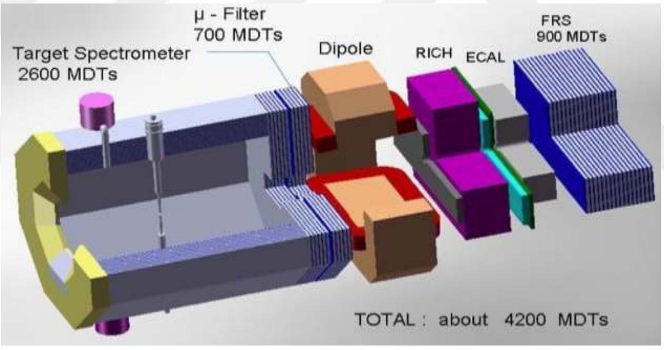

Figure 2.7. Muon System components of the PANDA Detector [25].

The thickness of the iron layers in the system is 3 cm. The gap width for MDTs is 3 cm. Each muon's high momentum is 6 cm thick and each muon has 16 rectangular iron plates. The muon dedector has an area of 3800×2565 mm^2 [26].

2.4.4 Muon Range System

The Muon Range System has the technique of detecting charged particles in the structure of gas detectors. Muon Range System (RS) structure is a known solution for detecting muons that pass through iron layers [27].

The average stopping power for high-energy muons in matter can be defined by <-dE/dX>=a(E)+b(E)E. Here, a(E) is the electronic stopping power and b(E) is the enegy scaled contribution from radiative process. a(E) and b(E) are slowly varying functions of the muon energy of the radiation effects [28].

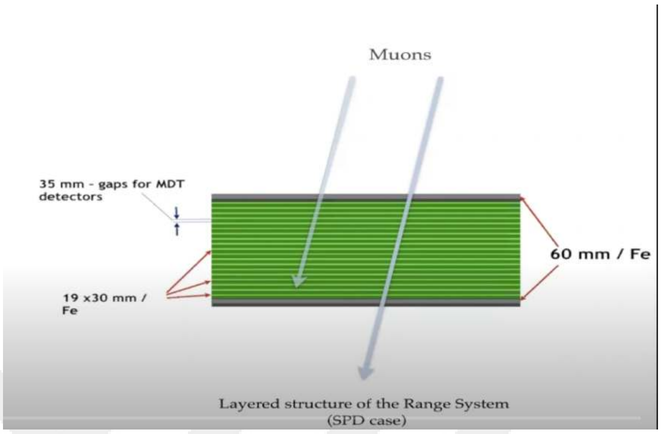

Figure 2.8. Schematic view of Muon Range System [27].

The geometric model of the prototype consists of four parts. Each part consists of 8-12 MDT detector layers (Figure 2.10). Each MDTs contains 8 elements, aluminum profiles and plastic envelope. There are 24 layers in total. The PANDA muon system uses a Range System (RS) technique to register muons in an iron absorber. Mini Drift Tubes (MDT) read two coordinate line information for charged particle detection in RS. [24].

2.4.5 Forward TOF (Forward Time of Flight)

Forward TOF is a particle description of low momentum hadrons. The TOF detector is proposed for the detection of low momentum particles moving left and right in the magnetic field inside the dipole [29].

The task of the FToF wall is to calculate the flight time of the forward particles emitted inside the FS in the laboratory below $5^0$and 10^0 in the vertical and horizontal directions. It has information on particle momentum and trace length provided by the dipole spectrometer equipped with a forward tracking system (FT).

The FToF wall hadrons (π, K, p *and their antiparticles*) should be defined in terms of time. Time of Flight information is obtained by time correlations between the responses of two or more scintillation counters of the FToF wall. So, it can use information of the FToF wall and Barrel TOF. For a relativistic particle, the flight time from the interaction point to the FToF wall location is approximatelly 25+Δ ns (Δ represents the type of particle) [29].

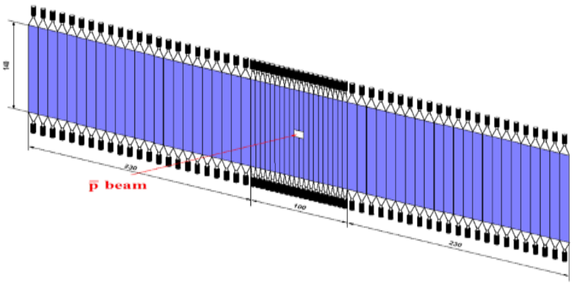

Figure 2.9. A schematic of the forward time-of-flight (FToF) scintillation wall placed 7.5 meters below the target in the Forward Spectrometer of the PANDA experiment. This diagram details the design and performance of the FToF wall detector [29].

The detector is composed of plastic scintillation sheets with good timing properties and fast Photomultiplier Tubes (PMT) reading (Figure 2.9). The counters create a precision wall 7.5 m below the target. The wall consists of 66 scintillation counters. There are 20 counters in the middle and 46 counters on the sides. The height of all plastic scintillator plates is 140 cm, their thickness is 2.5 cm, the width of the plates is 5 cm in the middle and 10 cm in the side [29].

2.4.6 Luminosity Monitor Detector

Luminance is an important parameter used in the collider experiments to normalize event statistics and determine physics potential. Luminance dedector is the most downstream PANDA dedector. The Luminance Monitor Detector (LMD) is the flow detector in the PANDA installation [30].

The luminosity in PANDA is different from the classical mechanicsm. Every outcome has a probability. In order to reduce the systematic uncertainty arising from the hadronic of the elastic scattering model, the measurement is made at low momentum transvers with a Coulomb cross section. Equivalent luminance must be determined to have an uncertainly more than 5%. The instantaneous relative luminance should be observed during the physics study [30,14].

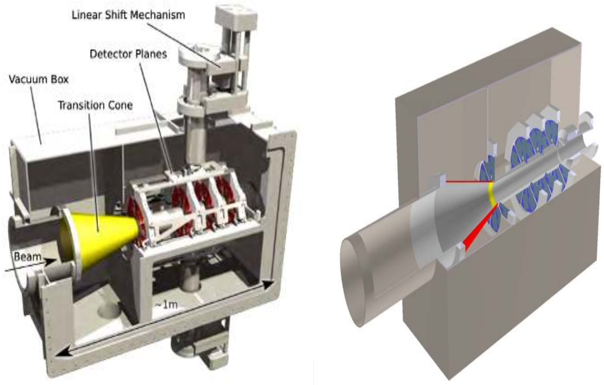

Figure 2.10. (Left) Side view of the luminosity dedector and (Right) Simulation view [30].

The setup of the LMD is shown in Figure 2.10. The LMD is approximately 10.5 m-12.5 m behind the target measuring at an angle range of 3 mrad to 9 mrad. The LMD vacuum box is observed at the beam tube passage from 70 mm diameter to 200 mm diameter. After the particles enter the LMD vacuum, they will pass through 4 detectors planes [30].

2.4.7 FTS (Forward Tracking System)

Forward Tracking System (FTS) is used for momentum analysis of charged particles around PANDA dipole magnet. The FTS measures the momentum of the particles depending on the deflection of their trajectories in the magnetic field of the PANDA dipole magnet. An algorithm for 3D tracking is presented in the Forward Tracking System part of the PANDA experiment. This tracker has addressed pipette tube detectors. The algorithm uses the trace path method when selecting trace candidates. The trace method applied consists of line, circle along the bending plane before and after the dipole magnet cavity. If there is an unbending plane, the projection is indicated by a straight line. The algorithm tests simulated muon traces, showing the results of trace finding efficiency and momentum results [31].

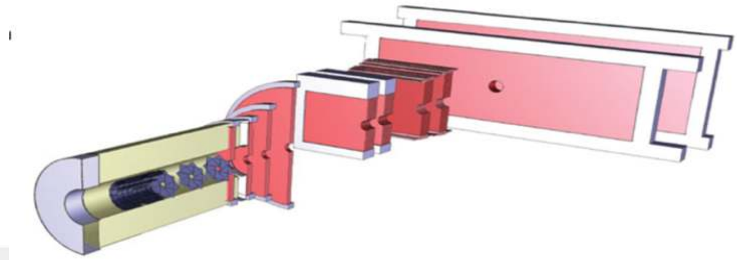

Figure 2.11. Schematic view of Forward Tracking System [32].

PANDA Forward Tracking System (FTS) is based on pipette tube detectors. The detection planes are made of modules of 32 pipettes in two layers. The FT is based on detectors with a 10 mm diameter tube. Each module is equipped with its own preamplifier-discriminatorcard [31].

2.4.8 GEM (Gas Electron Multiplier) Detector

Gas electron multipliers of high radiation doses and high indicator ratios in the CMS muon system complement have detectors in the beam tube. Like other CMS muon subsystems, GEMs have gas detectors. CMS GEMs are the first GEM rooms to be large in size and the largest GEM system installed. GEM system renews measurement of polar muon bending angle and deals with high rates of trigger of muon system [33].

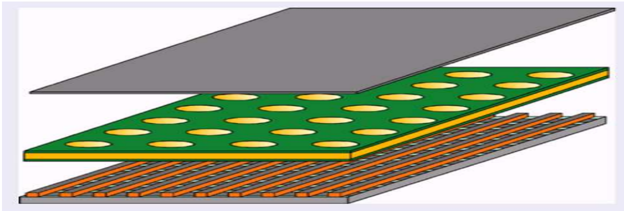

Figure 2.12. Schematic view of GEM (Gas Electron Multiplier) Detector [34].

GEMs are a fine insulation mesh with a diameter of 50 μm that separates two metal grids. Very high gain is obtained from the metal micro-mesh electrode with gaps in the range of 50 to 100 μm (Figure 2.12) [35].

2.4.9 STT (Straw Tube Tracker)

Straw Tube Tracker is a straw tube and a single channel drift tube. It is a gas filled tube with a wire along th eaxis. A high voltage of some kV is applied between the wire and the tube such that an electric field is present in the gas filled area. Ionization occurs in the particle pipette tube. Ions move toward the wall, electrons move toward the wire. The charge collected is proportional to the particle energy dissipated by the ionization. As a result, the electrical signal is allowed to be read. The basic module is known as a double layer tube to resolve the left and right uncertainty in the line relative to the wire. Regarding gas selection, a compromise must be made between the material budget and spatial resolution to minimize scattering [36].

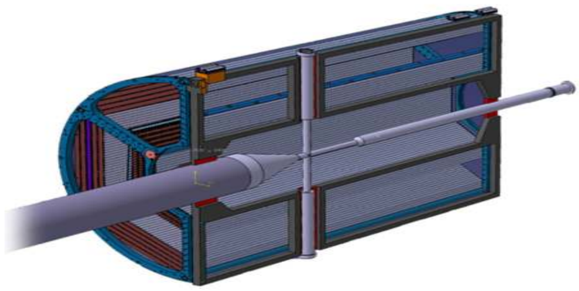

Figure 2.13. Image of tracking detectors of the Target Spectrometer [36].

The PANDA Straw Tube Tracker (Figure 2.13) is a piece of 150 cm long drift tubes cylindrical around the beam axis [36].

2.4.10 Forward Shashlyk EMC

The PANDA FS EMC is approximately seven meters below the antiproton – target interaction point. Used to detect electrons and positrons with energies of 10 MeV to 15 GeV. Hovewer, fast signal is required for a good energy resolution of EMC up to 10 GeV. One of the most interesting methods that meets this requirement and has the advantage of low cost is the fine segmentation Shashlyk calorimeter [37].

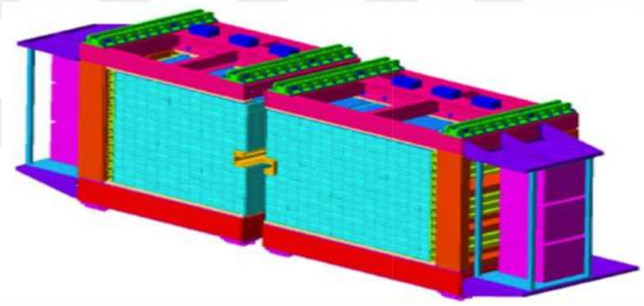

Figure 2.14. Schematic drawing of the Forward Shashlyk EMC [37].

The modules consist of 380 alternating layers lead and scintillator plate. The scintillation light is an optical fibers of 1.2 mm diameter. Each fiber is in a loop front of the module along the longitudinal axis of the module. The radius of the loop is 28 mm (Figure 2.14) [37].

3. AIM OF SCOPE OF THE STUDY

One of the physics motivation of PANDA experiment is to investigate charmonium-like particles, taking into account the PANDA experimental conditions and the environment. In this thesis, observation of exotic $Z_c(3900)^-$ particle is investigated with the experimental condition of PANDA experiment. In order to reach this goal, official software framework of PANDA experiment is used to generate the decay tree and fully simulated PANDA dedector is included. The mass and with of the $Z_c(3900)^-$is obtained with different fits (Gauss, Breit-Wigner and Voigt) and compared to those reported in the Particle Data Group (PDG). Some of the kinematic distributions of $Z_c(3900)^-$ particle are also given.

4. MATERIALS AND METHODS

4.1 PANDA Software Framework

The software framework used for the PANDA experiment is called PandaRoot. PandaRoot is a working platform designed for full simulation, reconfiguration and analysis of panda. The software version is advanced for simulation, particle identification and particle analysis. The PandaRoot framework (see Figure 4.1) is part of the FairRoot project, a common software framework for future FAIR experiments. It based on ROOT and Virtual Monte Carlo (VMC) packages. The FAIR facility is currently used to simulate detector performances and evaluate different detector concepts [38].

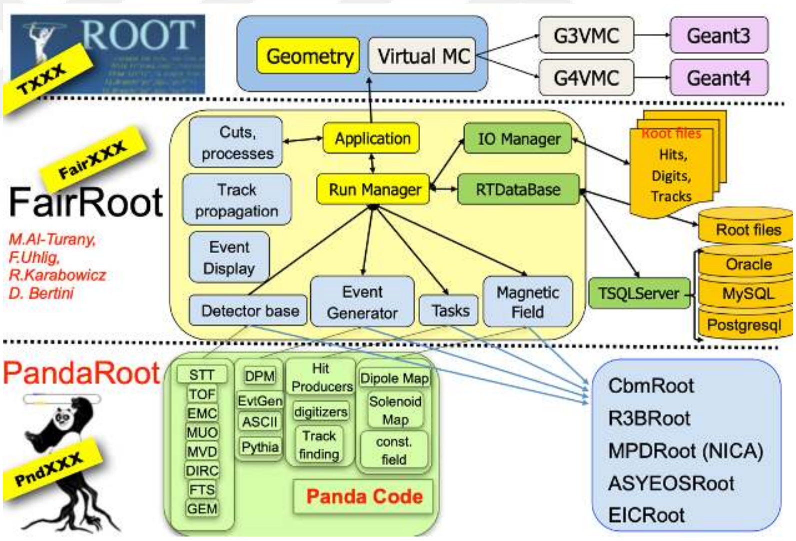

Figure 4.1. Schema is the structure of PandaRoot. Shown above are ROOT and Virtual Monte Carlo. The following step shows the overall infrastructure with PandaRoot framework simulation and task [38].

PandaRoot is under development and there are new versions regularly that bring improvements. The PANDA experiment at the future FAIR facility will observe anti-proton proton and anti-proton nucleus collisions in a beam momentum range from 2 GeV/c to 15 GeV/c. The PandaRoot framework is part of the FairRoot project. PANDA detector includes simulation code implementation and reconstruction code. These codes are implemented in all future FAIR experiments within the FairRoot software framework developed by GSI-IT. FairRoot itself also provides dynamic data structures with ROOT package in mind and virtual Monte Carlo (VMC) manages detector simulation. Therefore, GEANT3 and GEANT4 carry models can be used with the same detector code. GEANT3 and GEANT4 are based on ROOT and Virtual Monte Carlo packages. This facility is under development and optimization of different reconstruction algorithms for tracking and particle identification, meeting the performance requirements of the experiment. First, an initial track fitting is performed at the central tracker using a similar map transformation for a helix assumption. Then, the trace is used as input for a Kalman Filter (packed genfit) using the GEANT package as the tracer. The trace is associated with PID detectors to assess the probability of identifying a spherical particle using a Bayesian approach or multivariate methods. There are other packages implemented in PandaRoot Analysis tools framework Rho is a kinematic assembly package for peak, mass constraint fits and fast simulation code based on parameterized detector responses. Detector features and reconstruction code are developed in PandaRoot. Detector responses are simulated by digitizers. Events from tracking detectors are combined to create loaded traces. These are associated with PID detectors to generate charged candidates. Neutral candidates are formed from the electromagnetic calorimeter not associated with traces. Different particle identification algorithms assign particle probability to each candidate. So, the usersends particle identification feature to analysis. Few events are created in PandaRoot. EvtGen, DPM, Ultra Relativistic Quantum Molecular Dynamics (UrQMD), Pyhtia and Fluka are used for generation of physics and background events. These events are sent by the Virtual Monte Carlo (VMC) to transport model. The detector's geometry can be defined by American Standard Code for Information Intercharge (ASCII) files or ROOT objects. Additional opplication allows conversion of Computer Aided Design (CAD) drawings to ROOT geometries. Different particle identification algorithms send a particle probability to each candidate. So, the user selects her particle identification criteria and sends it to analysis. After simulation of events and propagation by detector, it is designed by the digitizers as a result of the detector [38].

The PandaRoot framework will be used for Monte Carlo studies and future data analysis. One of the goals of PandaRoot is that the code collaboration can be easily set up and used by most participants. PandaRoot simulations consists of five different steps as in Tablo 4.1 [38].

Table 4.1. Standard restructing scheme in PandaRoot [39].

MC Simulation
Digilitization
Event Reconstruction
Particle Identification
Event Analysis

4.1.1 Event Generation

The EvtGen [40] generator was designed to study physics process with B-meson distrubitions in B-factories. It provides the ability to handle and resonate complex sequential decay events. Particle reactions are investigated in high energy nuclear and particle physics. First of all, the first path we will follow is event generation. Event generation regulates the reactions studies learn about Hadron physics. Information about reconstructed particle tracks from tracking detectors is compared with information from PID detectors to generate charged candidates.

In this event; polarization, angular distribution, decay properties, decay modes are determined by the user. Simulation is required to evaluate the efficiency and accuracy of the detector in a given physics situation.

4.1.2 Digitization

Digitization is the second step of the simulation. The simulation examine the interaction and decay events (interaction point, energy loses…) with the PANDA detector. Digitization models signals to be processed in the front-end electronics of individual detectors and produce a digitized detector response similar to real data. It allows propagation using GEANT3 or GEANT4 transport codes. Digitizing signals, detector processing, produce digitized detectors close to real data are models.

4.1.3 Event Reconstruction

The PANDA experiment studies the collision of anti-proton beams with energy ranges between proton and nuclear targets with momentum between 2-15 GeV/c. PANDA detector features and reconfiguration code are implemented in PandaRoot. Particle identification algorithms are compared with Multivariate Analysis Methods.

The momentum value and corner coordinates of the charged particle are the interaction point (GEM) stations for the forward point with Micro Vertex Detector (MVD) covering Gaseous Electron Multipliers (GEM) by combining the information from the tracking detectors. The momentum and energy of the photons are reconstructed with electromagnetic calorimetry (ECM) subdetectors. Straw Tube Tracker (STT) beam is cylindrical around the axis. This section reconstructs the electromagnetic calorimetry subdetectors of photon. The continuous feld created by the incoming photon electromagnetic in the scintillator modules of EMC is called the cluster. The energy accumulation and the location of all the scintillator modules in the cluster help the first photon the identify the four vectors.

4.1.4 Particle Identification

Fragments and covariances defined by a set of parameters are placed at different positions in the spectrometer using the GEANE follower. The loaded candidates complete the information about PID i.e dE/dx, Cherenkov angle, part variables in EMC, energy deposition EMC clusters. Several PID algorithms work in which probability density functions are calculated for each candidate. PID software is divided into different into two different parts. In the first stage, a separate definition is made for each detector. Probabilities are provided for the five particle hypothesis $(e, \mu, \pi, \kappa\ and\ p)$. Probabilities are uniquely normalized with the same fluxes for each particle type. The second step is the global PID algorithm, which brings together the information from all sub-detectors by appliying the standard probability method. The simulation study described in this project uses the PID information from the four subdetectors EMC, STT (Barrel and Disk), DIRC and MVD for electron/pion separation.

4.2 Data Generation

The data for the study of $Z_c(3900)^-$particle has been produced with the DELL Server Computer which is located in the experimental particle physics laboratory at Bolu Abant İzzet Baysal University. Ubuntu 20.04.2 is running in the DELL Server which has 64 CPUs, 128 GB of RAM and 72 TB of storage. FairSoft vJun19p2, FairRoot-v18.2.1, PandaRoot-Developer version, GEANT4 and Root-v6.16/00 programs are installed and used for producing of signal and background events. Analysis has been done with a personal computer in which some version of the software and programs are running.

4.2.1 Event Generator

There are several event generators for simulating particle decays in high energy physics experiments. The EvtGen package provides a framework for new decays. When the degradation simulation takes place we call these modules EvtGen models. One of the purposes of EvtGen design is to use distortion amplitudes instead of probabilities to simulate distortions. In these days, the EvtGen framework models all decay distributions while applying only the nodes of the decay event. The EvtGen generator was selected by BaBar, CLEO, D0 and Belle collaborations. EvtGen is a Monte Carlo event generator that simulates the decays of heavy particles, the B and D mesons. It contains a set of decay models for intermediate and final states involving scaler, vector and tensor mesons or leptons, photons and baryons.

The EvtGen generator uses the model for generation particles Phase Space (PHSP). PHSP averages the spins of the particles in the initial state and the particles in the final state. It is combination of J/ψ and π^- particle to reconstruct $Z_c(3900)^-$ particle for electron and muon channels. Also, Vector Like Lepton (VLL) is used for final state particles in this generator.

4.2.2 Decay Scheme

One of the talismanic processes planned to be produced is to observe the $Z_c(3900)^-$ particle. The decay channels planned in the $Z_c(3900)^-$ particle and selected in the PANDA detector spectrometer for signal event generation are shown below. Using the Phase space of the PHSP model (flat distribution in the Center of Mass System (CMS)) 1 Million events are generated for the reaction at the value of antiproton momentum.

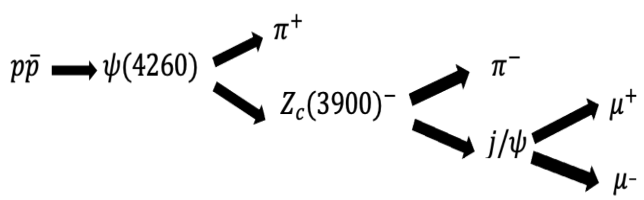

Figure 4.2. This virsual is the decay scheme used for $Z_c(3900)^-$generation in μ^+ and μ^- channels.

In order to produce in EvtGen generator, the decay channels must be introduced to program with the ".dec" file. There are four end state particles (μ^+, μ^-, π^+, π^-) three resonance particles ($\psi(4260)$, $Z_c(3900)^-$, j/ψ) in the dec file written to observe the $Z_c(3900)^-$ particle in Figure 4.2.

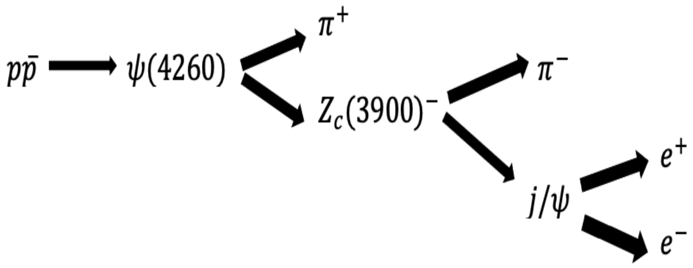

Figure 4.3. This virsual is the decay scheme used for $Z_c(3900)^-$generation in e^+ and e^- channels.

As explained above, the definition of the signal decay stagel to be produced in the electron channel to the EvtGen generator is defined by the ".dec" file. There are four end state particles (e^+, e^-, π^+ , π^-) three resonance particles ($\psi(4260)$, $Z_c(3900)^-$, j/ψ) in the dec file written to observe the $Z_c(3900)^-$ particle in Figure 4.3.

I would like to talk about the important points to be considered while writing the ".dec" file. In the ".dec" file, the decay entry begins with the word "Decay" and ends with the word "Enddecay". Capitalization is important in the decay table. Decay channel entries are leaves by ";". The charge conservation will be checked in the decay table. Each parent and daughter particle must be contained in the evt.pdl.

```
noPhotos

Decay pbarpSystem1
   1.0 Z_c(3900)- pi+ PHSP;
 Enddecay

Decay Z_c(3900)-
  1.0   J/psi pi-       PHSP;
Enddecay

Decay J/psi
  1.0   mu+ mu-         VLL;
Enddecay

End
```

Figure 4.4. $Z_c(3900)^-$is the ".dec" file prepared for signal event generation in the μ^+ and μ^- channels.

```
noPhotos

Decay pbarpSystem1
   1.0 Z_c(3900)- pi+ PHSP;
 Enddecay

Decay Z_c(3900)-
  1.0   J/psi pi-       PHSP;
Enddecay

Decay J/psi
  1.0   e+ e-       VLL;
Enddecay

End
```

Figure 4.5. $Z_c(3900)^-$is the ".dec" file prepared for signal event generation in the e^+ and e^- channels.

These two files are decay files that contain information about what degradation action should be taken. As seen in the decay file examples in Figure 4.4 and Figure 4.5 , the reconstructed particles $Z_c(3900)^-$ and J/ψ particles are resonance while particles π^+, π^- ,e^+, e^-, m^+, m^- are the particles observed in the spectrometer of the panda experiment. 1 Million signal events were generated with the EvtGen generator using the above decay files.

After the steps applied in PandaRoot, the data was applied to the analysis code of the C++ version. After the above steps in the analysis code, "*_par.root" and "_pid.root" files were applied as inputs. Defined PndAnalysis provides us some convenience to access data with PID (particle identification) selection. In this way, fetching objects from input files is done by FairRootManager via FairRunAna. We need muon candidates to reconstruct $J/\psi \longrightarrow \mu^+ \mu^-$ decay and electron candidates to reconstruct $J/\psi \longrightarrow e^+e^-$ decay. PbarpSystem1 is regenerated from one candidate and two oppositely charged pion candidates. Without using PID, all candidates are tuned to a certain mass hypothesis. A particle containing all positively and negatively charged particles with the mass hypothesis the list is created with the PndAnalysis::FillList method.

4.2.3 Beam Setup

The energy of $\psi(4260)$ particle converted from center of mass frame to laboratory frame by the following calculations in this section. When calculating, we took the mass of the $\psi(4260)$ particle as 4.230 GeV. In the calculating, m_1 and m_2 are the mass of the proton. Since m_1 and m_2 represent protons, the masses are equal.

$$E_{CM}=\sqrt{m_1^2 + m_2^2 + 2E_{1lab}m_2} \tag{4.1}$$

$$(E_{CM})^2=(\sqrt{m_1^2 + m_2^2 + 2E_{1lab}m_2})^2$$

$$E_{1lab} = \frac{{E_{CM}}^2 - m_1^2 - m_2^2}{2m_2}$$

$$E_{1lab} = \frac{(4.230\ GeV)^2-(0.938272\ GeV/c^2)^2-(0.938272\ GeV/c^2)^2}{2(0.938272\ GeV/c^2)}$$

$$E_{1lab}=8.59676 \text{ GeV/c}$$

If we want to calculate the proton beam, the following formula is applied. When we insert the energy value of the $\psi(4260)$ particle we find the value of the proton beam.

$$P_{beam} = \sqrt{E_{1lab}{}^2 - m_p^2} \tag{4.2}$$

$$P_{beam} = \sqrt{(8.59676\ Gev/c)^2 - (0.938272\ GeV/c^2)^2}$$

P_{beam}=8.5454 GeV/c

The energy calculation was made by writing the proton beam value found its place.

$$E_{CM} = \sqrt{(E_{\psi(2S)=4230})^2 + \vec{P}_{\bar{p}}{}^2} \tag{4.3}$$

$$E_{CM} = \sqrt{(4.230\ GeV)^2 + (8.5454\ GeV/c)^{2^2}}$$

E_{CM} =9.5350 GeV

The ".dec" file created in Figure 4.4 and Figure 4.5. runs on the EvtGen generator with the help of the "sh" shell command as seen in Figure 4.6. Phase Space (PHSP) model was used for these productions particles. The initial and final state radiation effects turned off with the simplification of analysis (noPhotons) commond. The aim is to make the analysis simple and to reduce the initial state radiation effect. The pbarpSystem1 particle has a mass of 5.50±0.24 GeV/c and a spin of 1. While performing the $p\bar{p}$ collision at the center of mass energy (4.230 ±

0.055 GeV/c) of the $\psi(4260)$ particle, the pbeam momentum was calculated as 8.5454 GeV and the total energy as 9.5350 GeV. Consequently, when generating data with full simulation by using PandaRoot, the momentum value (pbeam) of the $Z_c(3900)^-$particle was chosen as 8.5454 GeV/c according to calculations above in (4.1), (4.2) and (4.3).

4.2.4 Production Scripts

When producing data with PandaRoot, the program must read a shell script file to get information about the data that will be produced. This example shell script in Figure 4.6 which PandaRoot reads some parameters such as antiproton beam energy, decay file and number of events as well as includes “sim.C” macro that does full detector simulation when executed.

```
#!/bin/bash
#. ../../../build/config.sh
nev=10000
prefix="signal" # signal | bkg

if [[  "$prefix" == "signal"  ]];  then
prefix="signal_pp_Zc3900Minus_mumu"$nev
inputDecFile="pp_Zc3900Minus_mumu_nophot.dec"
elif [[  "$prefix" == "bkg"  ]]; then
prefix="dpm_pp_Zc3900Minus_mumu"$nev
inputDecFile="dpm_pp_Zc3900Minus_mumu"
fi

pbeam=8.5454
geantVersion="TGeant4"

if test "$1" != ""; then
  nev=$1
fi

if test "$2" != ""; then
  prefix=$2
fi

if test "$3" != ""; then
  input=$3
fi

if test "$4" != ""; then
  pbeam=$4
fi

if test "$5" != ""; then
  geantVersion=$5
fi

root -l -b -q  tut_sim.C\($nev,\"$prefix\",\"$inputDecFile\",$pbeam\,\"$geantVersion\"\)
root -l -b -q  tut_aod.C\($nev,\"$prefix\"\)
```

Figure 4.6. Shell script for $Z_c(3900)^-$ particle signal event generation.

The ‘’decay’’ file in Figure 4.4 and in Figure 4.5 are read to the EvtGen generator with the help of a shell script as in Figure 4.6. Signal event generation with 1 Million event number is done using Phase Space (PHSP) model for resonance particles and Vector Like Lepton (VLL) model for end state particles. By using the noPhotos command in production, it is aimed to reduce the initial state radiation effects and simplfiy the analysis, similar to the $Z_c(3900)^-$ particle.

4.2.5 Analysis

The produced data by using the determined decay channels were analyzed with the ROOT program. Analysis codes were written in PandaRoot libraries in order to perform this analysis. Particle identification (PID) of the generated data with the help of learned software and restructuring the masses of the particle by passing through various cuts were carried out.

The PID concept of PandaRoot software works as follows

-The tracked particle is reconstructed

-This trace is mopped to the PID detector signal

-The acquired PID information is reconstructed

-Probabilities are calculated for various particle types

All subdetector parts transmit probability information for PID to the main detector. “PID Combiner” defined to PandaRoot software combines similar probabilities from all detectors with the help of the following mathematical formula.

$$\tilde{P}_{tot,i} = \prod_{Det} P_{Det,i} \qquad i \in \{e, \mu, \pi, K, p\} \tag{4.4}$$

After this stage, the “PID Selector” becomes a particle identity deviation event. P_{tot} values that can reach possible amounts are selected. It depends on the sum of the information from the PID combiner. PID combiner and PID selector are objects in PandaRoot software. These are read to the software with the help of these objects.

PndAnaPidCombiner (Panda Analysis PID Combine Object): This combine calculates and combines all probabilities in various selection algorithms. These probabilities are populated into the RhoCandidate/RhoCandList candidate particle list.

PndAnaPidSelector (Panda Analysis PID Selector Object): This selector selects particles based on probabilities in the bonding object. "PndAnalysis::FillList" commond is used to pass both PID combiner and PID selector objects. If all muons and electrons in our analysis code are to be selected with the "FillList" commond, the following command is used.

```
analysis_Minus->FillList(muminus,"MuonAllMinus");
analysis_Minus->FillList(eminus,"ElectronAllMinus");
```

All muons and electrons in the data are passed through the PID selector to identify all probabilities as muons and electron candidates. In the PID combiner, these probabilities are combined and the candidate list is populated. For example; ''analysis_Zc3900'' refers for Panda analysis initializer, ''muminus'' is the name for all μ^- candidates and ''FillList'' command is the command which gathers information from the detector simulated data about that the candidate.

```
analysis_Zc3900->FillList(muplus,"MuonAllPlus");
analysis_Zc3900->FillList(muminus,"MuonAllMinus");
analysis_Zc3900->FillList(eplus,"ElectronAllPlus");
analysis_Zc3900->FillList(eminus,"ElectronAllMinus");
analysis_Zc3900->FillList(piplus,"PionAllPlus");
analysis_Zc3900->FillList(piminus,"PionAllMinus");
```

The data created in the collision simulation using the PandaROOT software is written to the PANDA detector signal ".root" file. The above analysis code selects all end state particles in the decay channel Figure 4.2 and Figure 4.3 for $Z_c(3900)^-$ analysis with this method. This method populates particle candidates into lists. While J/ψ is reconstructed, muons and electrons are chosen for the reconfigurations in this analysis study. The analysis code from comes the final state particles of the reconstructed J/ψ particle is as follows. Similarly, following the decay scheme $Z_c(3900)^-$ and $\psi(4260)$ particles are written.

Firstly, while the J/ψ particle was reconstructed, electrons and positrons were reconstructed in the analysis study. Then all the end state particles were selected with the help of software. After this stage, the analysis code written from which end state particles the J/ψ particle to be reconstructed comes from is indicated in the line below.

```
jpsi.Combine(muplus,muminus);
jpsi.SetType(443);
jpsi.Combine(eplus,eminus);
jpsi.SetType(443);
```

Then, after all electrons and positrons in Figure 4.2 and Figure 4.3 filled into the lists, ''Combine'' command was applied without applying any cutting by passing through PID combiner and PID selector. Similarly, $Z_c(3900)^-$ particle were reconstructed following the decay scheme.

```
Z3900Minus.Combine(jpsi,piminus);
Z3900Minus.SetType(-99010443);
Z3900Minus.Combine(jpsi,piminus);
Z3900Minus.SetType(-99010443);
```

Finally, $\psi(4260)$ particle were reconstructed like above. ''SetType'' command shows the particle numbers in the file named ''evt.pdl'', which is used by the software and contains various information about the particles.

```
pbarpPlus.Combine(Z3900Minus,piplus);
pbarpPlus.SetType(88881);
pbarpPlus.Combine(Z3900Minus,piplus);
pbarpPlus.SetType(88881)
```

Table 4.2. Example of particle numbering and information of found particles in file ''evt.pdg'' [41].

Name	ID	Mass(GeV)	Width(GeV)	Max Dm(GeV)	3* charge	2* spin	lifetime*C(mm)	PYTHIA ID
e^-	11	5.1099895e-04	0.0000000e+00	0.0000000e+00	-3	1	0.0000000e+00	11
e^+	-11	5.1099895e-04	0.0000000e+00	0.0000000e+00	3	1	0.0000000e+00	-11
μ^-	13	1.0565837e-01	2.9959847e-19	2.9959847e-18	-3	1	6.5864973e+05	13
μ^+	-13	1.0565837e-01	2.9959847e-19	2.9959847e-18	3	1	6.5864973e+05	-13
π^+	211	1.3957061e-01	2.5284000e-17	2.5284000e-16	3	0	7.8044971e+03	211
π^-	-211	1.3957061e-01	2.5284000e-17	2.5284000e-16	-3	0	7.8044971e+03	211
J/ψ	443	3.09690003+00	9.2900000e-05	9.2900000e-04	0	2	0.0000000e+00	443
$Zc(3900)^+$	99010443	3.8872000e+00	2.8200000e-02	2.8200000e-01	3	2	0.0000000e+00	99010443
$Zc(3900)^-$	-99010443	3.8872000e+00	2.8200000e-02	2.8200000e-01	-3	2	0.0000000e+00	-99010443
$\psi(4260)$	99100443	4.2300000e+00	5.5000000e-02	5.5000000e-01	0	2	0.0000000e+00	99100443

The above software line of code help contain various information about the particle's mass, width, charge and spin. Thus, reached particle enables us to reach the information of the particle to be reconstructed. The particles in the table were passed through the PID combiner and PID selector according to the decay scheme in Figure 4.2. and Figure 4.3. After selecting all the electrons and positrons in the list, the desired final state particles J/ψ, $Z_c(3900)^-$, $\psi(4260)$ particles were reconstructed with the "Combine" command without any cutting operation. The "SetType" command shows the particle numbers in the "evt.pdg" file that the software uses and contains various information about the particles. As above, we produced data for 1 Million events by reading the ".dec" file in the PandaRoot software to our code. Then, the additions to the analysis code in the tutorial codes, $Z_c(3900)^-$ invariant mass graps were obtained.

Table 4.3. The mass and width of J/ψ, $Z_c(3900)^-$, $\psi(4260)$ particles in the Particle Data Group (PDG) [41].

PDG Value	J/ψ	$Z_c(3900)^-$	$\psi(4260)$
Mass Value	3096.900±0.006 MeV	3888.4 ±2.5 MeV	4230±8 MeV
Width Value	92.9±2.8 keV	28.3±2.5 MeV	55±19 MeV

As shown in Table 4.3, the mass and width units are in keV and MeV. The units must be converted to GeV according to the calculations made.

Firstly, the mass of J/ψ particle is 3.096 GeV. Calculations were made by converting the mass error of the J/ψ particle from 0.006 MeV to 0.000006 GeV. The width of J/ψ particle is 92.9 keV and the error is 2.8 keV. Calculations were made by converting the width of the J/ψ particle from 92.9 keV to 0.0000929 GeV and the width error is 0.0000028 GeV. Secandly, the mass of $Z_c(3900)^-$ particle is 3.888 GeV. Calculations were made by converting the mass error of the $Z_c(3900)^-$particle from 2.5 MeV to 0.0025 GeV. The width of $Z_c(3900)^-$particle is 28.3 MeV and the error is 2.5 MeV. Calculations were made by converting the width of the $Z_c(3900)^-$ particle from 28.3 MeV to 0.0283 GeV and the width error is 0.0025 GeV. Finally, the mass of $\psi(4260),$ particle is 4.230 GeV. Calculations were made by converting the error of the $\psi(4260)$ particle from 8 MeV to 0.008 GeV. The width of $\psi(4260)$ particle is 55 MeV with an error of 19 MeV. Calculations were made by made converting the width of the $Z_c(3900)^-$ particle from 55 MeV to 0.055 GeV and the error is 0.019 GeV.

The mass and width values of J/ψ , $Z_c(3900)^-$, $\psi(4260)$ particles in the Particle Data Group (PDG) shown in Tablo 4.3. These values obtained as a result of experimental studies worldwide. The mass values reconstructed as a result of the analysis in this work are in good agreement with thosse values given in literature. The simulation of the PANDA detector integrated into the PandaRoot software has been successfully carried out. Three particles to be observed in the detector spectrometer can be reconstructed.

After the analyzes Tablo 4.1, various algorithms and cuts were applied for the selected $Z_c(3900)^-$ particle. It was aimed that the reconstruction would yield appropriate results. All of the selected and reconstructed particles have been passed through the above cuts. Firstly, the mass distribution was observed without applying any cuts. Choosing those above 1%, McTruthMatch (Monte Carlo Truth Match) was applied to eliminate all low mass candidates while reducing the values of the particle candidates. After applying a vertex Fit cut to find the peak position of the reconstructed particles, a mass constraint fit in the range of $\pm$ 0.3 GeV was applied to select the mass of the particles in accordance with the literature. As a result of these kinematic constraints and cut, the analysis results are close to the masses of the particles compared to the experimental results in the literature.

Secandly, the Gaussian Fit function is applied to show the statistical distribution. In the Gauss Fit formula (4.5) below; the a parameter is the curve vertex height, b is the center position of the vertex, c controls the width of the ‘’bell’’ .

$$f(x)=ae - \frac{(x-b)^2}{2c^2} \qquad (4.5)$$

Thirdly, the Breit-Wigner Fit function is used in high energy physics and applied for modeling resonant particles. In the Breit-Wigner Fit formula (4.6) below; E is the center of mass energy producing resonance, M is the resonance mass, Γ is the resonance of width and k is the proportionality constant.

$$f(E)=\frac{k}{(E^2-M^2)^2+M^2\Gamma^2} \qquad (4.6)$$

$$k=\frac{2\sqrt{2}M\Gamma\gamma}{\pi\sqrt{M^2+\gamma}}$$

$$\gamma = \sqrt{M^2(M^2+\tau^2)}$$

Fourthly, the probability distribution formed by the combination of a Voigt Fit Cauchy-Lorentz distribution and a Gaussian distribution is applied.

Fifthly, TLorentzVector is an implementation of four vectors for position and time (x,y,z,t) or momentum and energy (Px, Py, Pz, E). These four vector classes are P_T, Eta, CosTheTa, Phi. In this analysis, P_T, Eta, and Phi distributions were observed. The purpose of kinematic fit is to improve the resolution of experimental measurements and to find unknown parameters by minimizing the constrainst law of the physics.

Kinematic fit distributions are obtained as the initial vectors of the TLorentzVector (0, 0, 8.5454, 9.5350). The first value is the Px value and the second value is the Py value. When we insert the energy value of the $\psi(4260)$ particle, the value we find is the value of the proton beam. This value is indicated by Pz and this value is 8.5454. The energy value was found by calculating the beam of the proton with the value we found by converting from the center of mass frame to the laboratory frame. This value is indicated by E and this value is 9.5350. The values are obtained from the calculations (4.2) and (4.3).

In this analysis stage, the decay process for the $Z_c(3900)^-$ particle is determined and the $Z_c(3900)^-$ particle is reconstructed. As seen in Figure 4.2 and Figure 4.3, π^+, π^-, μ^+, μ^-, e^+, e^-particles are observed in the spectrometer of the PANDA experiment. Since the $Z_c(3900)^-$ particle is not defined in PandaRoot EvtGen, the file in Tablo 4.1 is added. The analysis code is written in C++ programing language which follows the decay scheme to reconstruct J/ψ, $Z_c(3900)^-$, $\psi(4260)$ particles respectively. Then, invariant mass distributions of J/ψ, $Z_c(3900)^-$, $\psi(4260)$ particles are obtained by various algorithm and cuts. The kinematic distributions of the reconstructed $Z_c(3900)^-$ particle are also observed. Finally, Gauss Fit, Breit-Wigner Fit and Voigt Fit is applied to invariant mass distributions. The analysis has performed for 1 Million events and results are discussed in the next section.

5. RESULTS AND DISCUSSION

This section mentions about the regeneration process of the last state particles J/ψ , $Z_c(3900)^-$ and $\psi(4260)$ particles. It also describes three different procedures for fitting the results obtained for each case to the invariant mass of e^+e^-or $\mu^+\mu^-$, $e^+e^-\pi^-$ and $e^+e^-\pi^+\pi^-$.

The reconstructed flowchart is shown in Figure 5.1. Firstly, the analysis begins with the reconstruction of the J/ψ particle in e^+e^- and $\mu^+\mu^-$ channel. Consequently, J/ψ particle is combined with π^- to regenerate $Z_c(3900)^-$ particle, while $Z_c(3900)^-$ particle is combined with π^+ to regenerate $\psi(4260)$ particle.

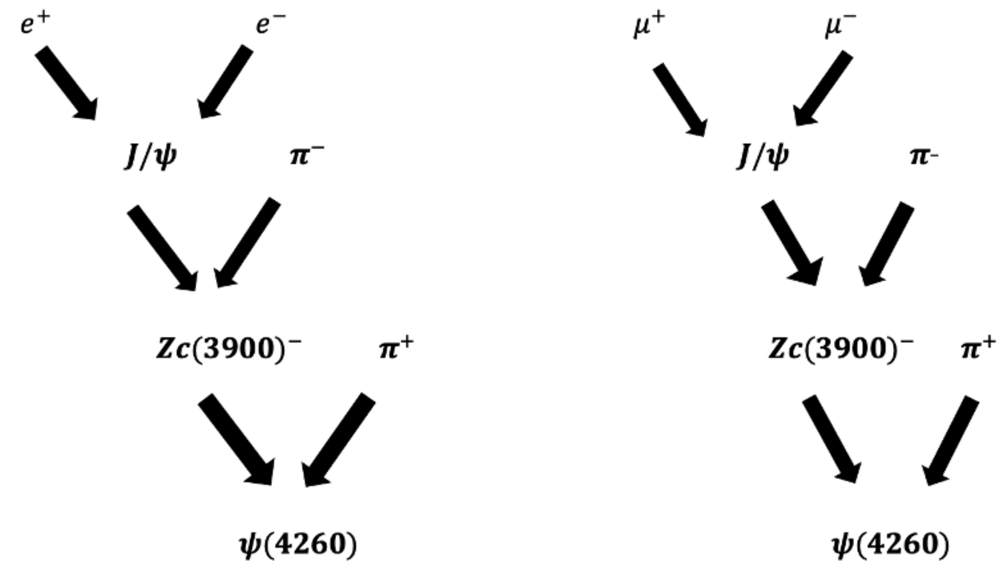

Figure 5.1. Flow chart for electron and muon channels for Z_c $(3900)^-$ particle.

At the same time, this section will discuss how the spectrometer observability of exotic states such as the Z_c $(3900)^-$ particle is designed and optimized from the perspective.

The analysis begins by applying the selection algorithm steps. Firstly, Rough Mass Selection is applied to the fraction containing the reconstructed particle candidates The secand stage is the Full Truth Match cut application. This algorithm is the particle identification class by performing Monte Carlo accuracy matching.

Third, the cut application that brings the particle traces in the signal closer to the corner points are called Vertex Fit. When applying this cut, more than 1% is selected. The final stage is the application of Mass Constraint Fit. All low mass candidates are eliminated while lowering the values of the particle candidates by selection those above 1%. Gauss Fit is applied to statistically see the invariant mass distribution after the Mass Constraint Fit function. After the Mass Constraint Fit stage, we applied Gaussian fit to see the mass distributions statistically. Then, by applying the Breit-Wigner Fit function to the J/ψ, $Z_c(3900)^-$, $\psi(4260)$ particle, it is observed how close the mass values of the particles can be to the values in the literature. After the Mass Constraint Fit stage, the next step for position, time, energy and momentum definition is Kinematic Fitting.

As a result, we examined the data analysis results obtained within the scope of the PANDA Collaboration and all phenomenologic studies related to particle physics.

5.1 Reconstruction of J/ψ Particle

Not only the effects of different selection criteria but also Gauss Fit, Breit-Wigner Fit and Voigt Fit results to the distribution of invariant mass of μ^+, μ^- or e^+, e^- are discussed. Distribution of Kinematic variables for the reconstructed J/ψ particles are also presented.

5.1.1 $\mu^+\mu^-$ Channel

The J/ψ particle candidates are reconstructed by combining the μ^+ and μ^- candidates. The invariant mass distributions and kinematic valuable of the reconstructed J/ψ particle candidates are observed.

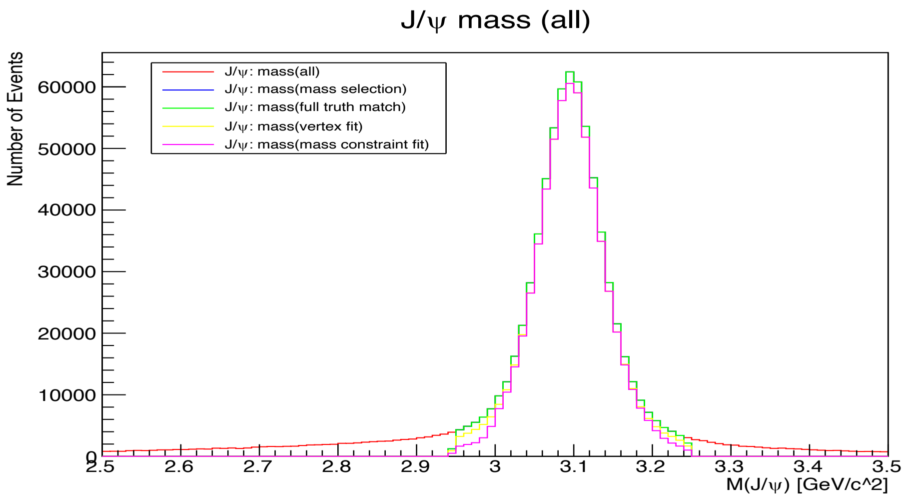

Figure 5.2. The invariant mass distributions of the J/ψ particle candidates reconstructed by μ^+ and μ^- after aplying different selection creteria.

In Figure 5.2, the invariant mass distributions of the J/ψ particle candidates reconstructed by μ^+ and μ^- is plotted in the range of 2.5-3.5 GeV/c^2 for different selection creteria to see the efect of it. Red line representes the events where all combinations of μ^+ and μ^- combined to reconstruct J/ψ particle in the given range. 910829 events out of 1 Million have reconstructed J/ψ particle in this range which leads to the efficiency rate of 91%. Blue line represents the J/ψ particle candidates after the Mass Selection cut which is $\pm$ 0.15 GeV/c^2 around the mass of J/ψ particle 3.095 GeV/c^2 reported in PDG. 684896 events out of 1 Million have reconstructed J/ψ particle in this range which leads to the efficiency rate of 68.4%. The green line represents the J/ψ particle candidates after the McTruthMatch algorithm was applied. 684823 events out of 1 Million have reconstructed J/ψ particle in this range which leads to the efficiency rate of 68.4%. The yellow line represents the J/ψ particle candidates after the Vertex Fit algorithm was applied with more than 1% probability. 644768 events out of 1 Million have reconstructed J/ψ particle in this range which leads to the efficiency rate of 64.4%. The pink line represents a large reduction in the number of J/ψ particle candidates after Mass Constraint matching. 628336 events out of 1 Million have reconstructed J/ψ particle in this range which leads to the efficiency rate of 62.8%.

As can be seen in Figure 5.2, the invariant mass distributions of each particle in the decay chain are gradually restricted after each cut. It is seen that the peak in the desired mass range is sharpened and this peak approaches the mass of the J/ψ particle to be reconstructed.

In order to obtain mass and width of J/ψ particle, three different fit function has been applied. First of all, Gauss Fit is applied to the reconstructed mass distribution of μ^+ and μ^- system after Mass Constraint Fit. Mass and width are obtained for mass and width of J/ψ particle, respectively. When Breit-Wigner Fit is performed to the same distribution, mass and width are obtained. Finally, Voigt Fit gives better than other fits.

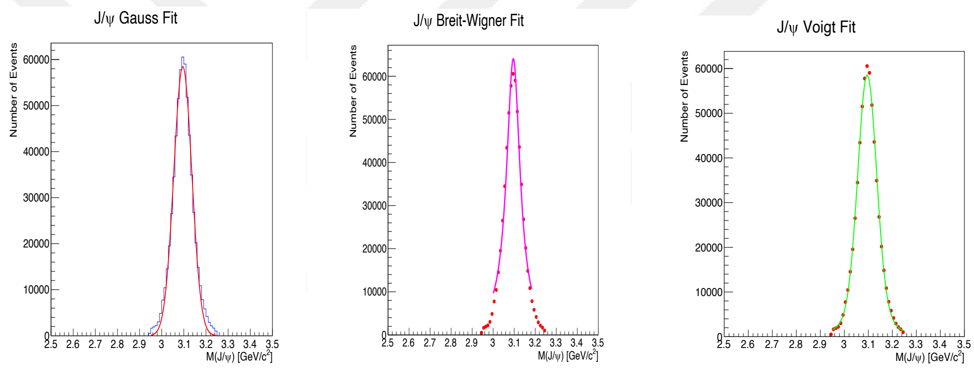

Figure 5.3. The distribution of the mass values obtained for J/ψ particle reconstructed from μ^+ and μ^- after the Mass Constraint Fit: Gauss Fit, Breit-Wigner Fit and Voigt Fit from left to right, respectively.

According to the first graphic in Figure 5.3, the red line represents the Gauss Fit distribution applied to the J/ψ particle candidates reconstructed in the range of 2.5-3.5 GeV/c^2. The mass value is 3.095 GeV and the width value is 0.09588 GeV after applying Gaussian Fit to J/ψ particle. These mass and width values are known as 3.096 GeV and 0.0000929 GeV in the literature, respectively. When mass values are compared, the value in the literature is 99.96% with an error rate of 0.032%. According to the secand graphic, the pink line represents the Breit-Wigner Fit Fit distribution applied to the J/ψ particle candidates reconstructed in the range of 2.5-3.5 GeV/c^2. The mass value is 3.097 GeV and the width value is 0.07902

GeV after applying a Breit-Wigner Fit to J/ψ particle. When mass values are compared, the value in the literature is 99.96% with an error rate of 0.032%. According to the third graphic, the green line represents the Voigt Fit distribution applied to the J/ψ particle candidates reconstructed in the range of 2.5 - 3.5 GeV/c^2. The mass value is 3.096 GeV and the width value is 0.03492 GeV after applying a Voigt Fit to J/ψ particle. When these results in the distribution are compared, the mass value is the same as in the PDG value. 628336 events out of 1 Million have reconstructed J/ψ particle in this range which leads to the efficiency rate of 62.8%.

In order to obtain kinematic functions of J/ψ particle, three different distribution has been applied. First of all, P_T distribution is applied to the reconstructed mass distribution of μ^+ and μ^- system after Mass Constraint Fit. After the P_T distribution, the Eta distribution from the kinematic functions of the J/ψ particle is applied. The final kinematic function of J/ψ particle is applied to the Phi distribution.

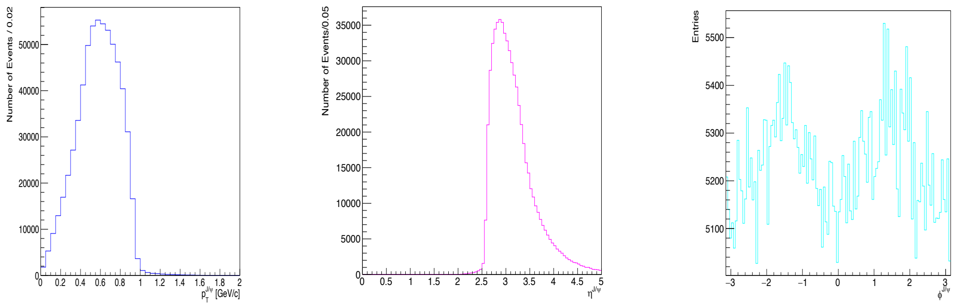

Figure 5.4. The distribution of kinematic variables of J/ψ particle reconstructed from μ^+ and μ^- after the Mass Constraint Fit: $P_T^{J/\Psi}$ (Transverse momentum) distribution, $\eta_T^{J/\Psi}$ (Eta) distribution and $\phi_T^{J/\Psi}$ (Phi) distribution from left to right, respectively.

Three different distributions are applied to obtain the kinematic values of the J/ψ particle. In the graph on the left, the Transverse momentum distribution of J/ψ particle with a peak of 0.57 GeV/c in the range of 0-2 GeV/c is obtained. In the middle graph, the Eta distribution of J/ψ particle with a peak of 3.16 in the range of 0-5 is obtained. In the right graph, the Phi distribution of J/ψ particle with a peak of 0.0001874 in the range of -3 and 3 is obtained. 628336 events out of 1

Million have reconstructed of J/ψ particle on P_T, Eta, Phi distribution which leads to the efficiency rate of 62.8%.

5.1.2 e^+e^- Channel

The J/ψ particle candidates are reconstructed by combining the e^+ and e^- candidates. The invariant mass distributions and kinematic valuable of the reconstructed J/ψ particle candidates are observed.

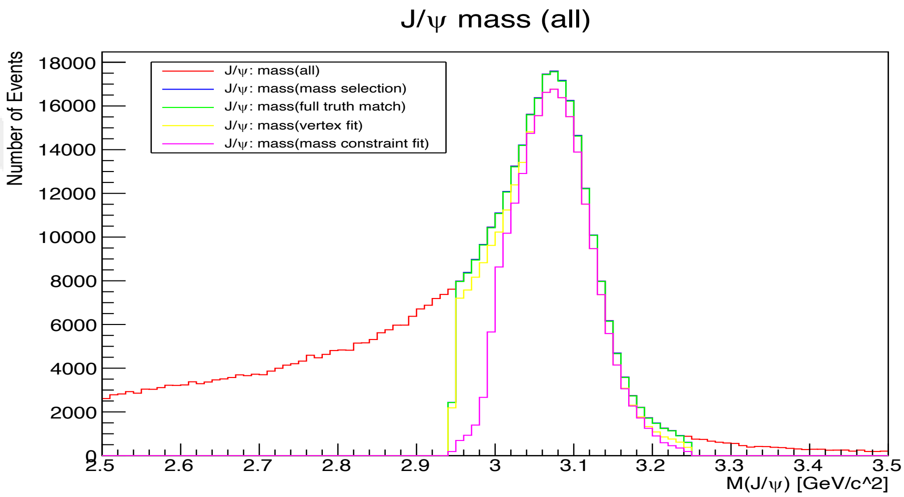

Figure 5.5. The invariant mass distributions of the J/ψ particle candidates reconstructed by e^+ and e^- after aplying different selection creteria.

In Figure 5.5, the invariant mass distributions of the J/ψ particle candidates reconstructed by e^+ and e^- is plotted in the range of 2.5-3.5 GeV/c^2 for different selection creteria to see the efect of it. Red line representes the events where all combinations of e^+ and e^- combined to reconstruct J/ψ particle in the given range. 842427 events out of 1Milyon have reconstructed J/ψ particle in this range which leads to the efficiency rate of 84.2%. Blue line represents the J/ψ particle candidates after the Mass Selection cut which is $\pm$ 0.15 GeV/c^2 around the mass of J/ψ particle 3.096 GeV/c^2 reported in PDG. 270474 events out of 1 Million have reconstructed J/ψ particle in this range which leads to the efficiency rate of 27%. The green line represents the J/ψ particle candidates after the McTruthMatch algorithm was applied. 269834 events out of 1 Million have reconstructed J/ψ

particle in this range which leads to the efficiency rate of 26.9%. The yellow line represents the J/ψ particle candidates after the Vertex Fit algorithm was applied with more than 1% probability. 250663 events out of 1 Milyon have reconstructed J/ψ particle in this range which leads to the efficiency rate of 25%. The pink line represents a large reduction in the number of J/ψ particle candidates after Mass Constraint matching. 213123 events out of 1 Million have reconstructed J/ψ particle in this range which leads to the efficiency rate of 21.3%.

As can be seen in Figure 5.5, the invariant mass distributions of each particle in the decay chain are gradually restricted after each cut. It is seen that the peak in the desired mass range is sharpened and this peak approaches the mass of the J/ψ particle to be reconstructed.

In order to obtain mass and width of J/ψ particle, three different fit function has been applied. First of all, Gauss Fit is applied to the reconstructed mass distribution of e^+ and e^- system after Mass Constraint Fit. Mass and width are obtained for mass and width of J/ψ particle, respectively. When Breit-Wigner Fit is performed to the same distribution, mass and width are obtained. Finally, Voigt Fit gives better than other fits.

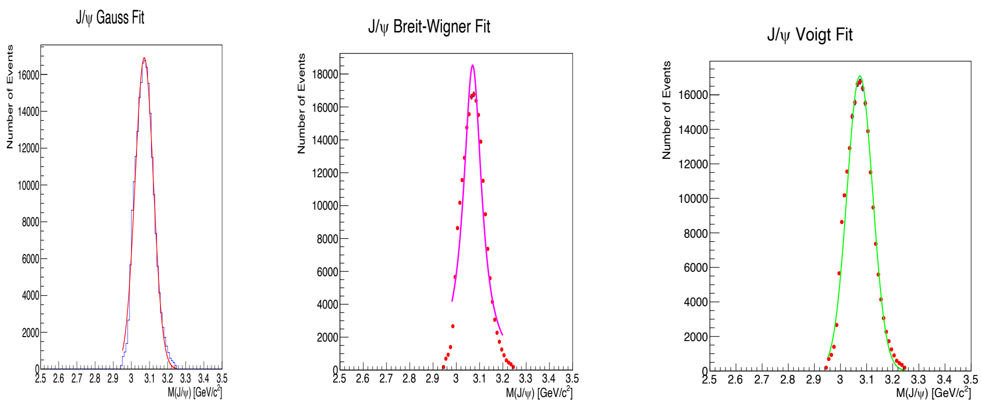

Figure 5.6. The distribution of the mass values obtained for J/ψ particle reconstructed from of e^+ and e^- after the Mass Constraint Fit: Gauss Fit, Breit-Wigner Fit and Voigt Fit from left to right, respectively.

According to the first graphic in Figure 5.6, the red line represents the Gauss Fit distribution applied to the J/ψ particle candidates reconstructed in the range of 2.5-3.5 GeV/c^2. The mass value is 3.071 GeV and the width value is 0.118158 GeV after applying Gaussian Fit to J/ψ particle. These mass and width values are known as 3.096 GeV and 0.0000929 GeV in the literature, respectively. When mass values are compared, the value in the literature is 99.19% with an error rate of 0.80%. According to the second graphic, the pink line represents the Breit-Wigner Fit Fit distribution applied to the J/ψ particle candidates reconstructed in the range of 2.5-3.5 GeV/c^2. The mass value is 3.072 GeV and the width value is 0.09437 GeV after applying a Breit-Wigner Fit to J/ψ particle. When mass values are compared, the value in the literature is 99.22% with an error rate of 0.77%. According to the third graphic, the green line represents the Voigt Fit distribution applied to the J/ψ particle candidates reconstructed in the range of 2.5-3.5 GeV/c^2. The mass value is 3.074 GeV and the width value is 0.04914 GeV after applying a Voigt Fit to J/ψ particle. When mass values are compared, the value in the literature is 99.28% with an error rate of 0.71%. 213123 events out of 1 Million have reconstructed J/ψ particle in this range which leads to the efficiency rate of 21.3%.

In order to obtain kinematic functions of J/ψ particle, three different distribution has been applied. First of all, P_T distribution is applied to the reconstructed mass distribution of e^+ and e^- system after Mass Constraint Fit. After the P_T distribution, the Eta distribution from the kinematic functions of the J/ψ particle is applied. The final kinematic function of J/ψ particle is applied to the Phi distribution.

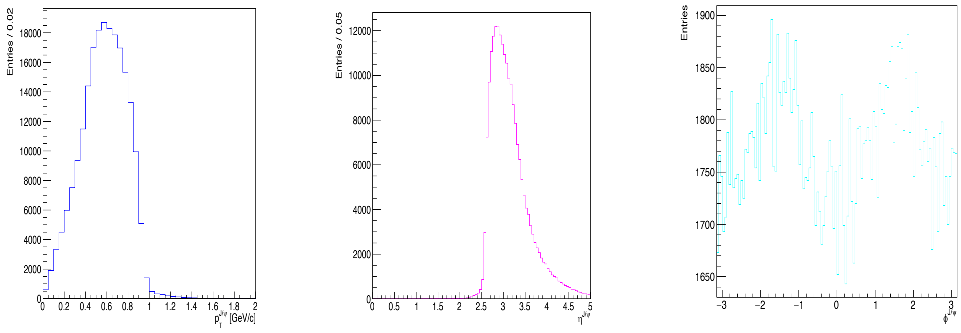

Figure 5.7. The distribution of kinematic variables of J/ψ particle reconstructed from $e^{+}$and e^{-}after the Mass Constraint Fit: $P_T^{J/\Psi}$(Transverse momentum) distribution, $\eta_T^{J/\psi}$ (Eta) distribution and $\phi_T^{J/\psi}$ (Phi) distribution from left to right, respectively.

Three different distributions are applied to obtain the kinematic values of the J/ψ particle. In the graph on the left, the Transverse momentum distribution of J/ψ particle with a peak of 0.57 GeV/c in the range of 0-2 GeV/c is obtained. In the middle graph, the Eta distribution of J/ψ particle with a peak of 3.15 in the range of 0-5 is obtained. In the right graph, the Phi distribution of J/ψ particle with a peak of 0.0025 in the range of -3 and 3 is obtained. 213123 events out of 1 Million have reconstructed of J/ψ particle on P_T, Eta, Phi distribution which leads to the efficiency rate of 21.3%.

5.2 Reconstruction of $Z_c(3900)^-$ Particle

Not only the effects of different selection criteria but also Gauss Fit, Breit-Wigner Fit and Voigt Fit results to the distribution of invariant mass of μ^{+}, μ^{-} or e^{+}, e^{-} are discussed. Distribution of Kinematic variables for the reconstructed $Z_c(3900)^-$ particles are also presented.

5.2.1 $\mu^+\mu^-$ Channel

The $Z_c(3900)^-$ particle candidates are reconstructed by combining the μ^+ and μ^- candidates. The invariant mass distributions and kinematic valuable of the reconstructed $Z_c(3900)^-$particle candidates are observed.

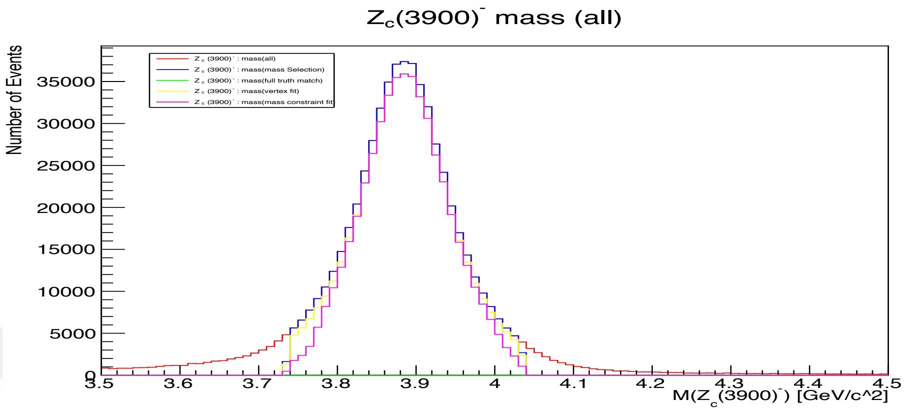

Figure 5.8. The invariant mass distributions of $Z_c(3900)^-$ the particle candidates reconstructed by μ^+ and μ^- after aplying different selection creteria.

In Figure 5.8, the invariant mass distributions of the $Z_c(3900)^-$particle candidates reconstructed by μ^+ and μ^- is plotted in the range of 3.5-4.5 GeV/c^2 for different selection creteria to see the efect of it. Red line representes the events where all combinations of μ^+ and μ^- combined to reconstruct $Z_c(3900)^-$ particle in the given range. 649351 events out of 1 Million have reconstructed $Z_c(3900)^-$ particle in this range which leads to the efficiency rate of 64.3%. Blue line represents the $Z_c(3900)^-$particle candidates after the Mass Selection cut which is ± 0.15 GeV/c^2 around the mass of $Z_c(3900)^-$ particle 3.888 GeV/c^2 reported in PDG. 556287 events out of 1 Million have reconstructed $Z_c(3900)^-$ particle in this range which leads to the efficiency rate of 55.6%. The green line represents the $Z_c(3900)^-$ particle candidates after the McTruthMatch algorithm was applied. 550574 events out of 1 Million have reconstructed $Z_c(3900)^-$ particle in this range which leads to the efficiency rate of 55%. The yellow line represents the $Z_c(3900)^-$ particle candidates after the Vertex Fit algorithm was applied with more than 1% probability. 523479 events out of 1 Milyon have reconstructed $Z_c(3900)^-$ particle in this range which leads to the efficiency rate of

52.3%. The pink line represents a large reduction in the number of $Z_c(3900)^-$ particle candidates after Mass Constraint matching. 498268 events out of 1 Million have reconstructed $Z_c(3900)^-$ particle in this range which leads to the efficiency rate of 49.8%.

As can be seen in Figure 5.8, the invariant mass distributions of each particle in the decay chain are gradually restricted after each cut. It is seen that the peak in the desired mass range is sharpened and this peak approaches the mass of the $Z_c(3900)^-$ particle to be reconstructed.

In order to obtain mass and width of $Z_c(3900)^-$ particle, three different fit function has been applied. First of all, Gauss Fit is applied to the reconstructed mass distribution of μ^+ and μ^- system after Mass Constraint Fit. Mass and width are obtained for mass and width of $Z_c(3900)^-$ particle, respectively. When Breit-Wigner Fit is performed to the same distribution, mass and width are obtained. Finally, Voigt Fit gives better than other fits.

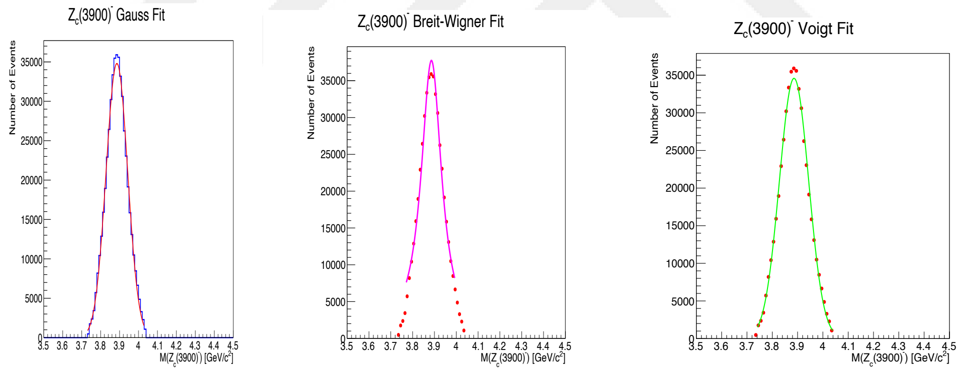

Figure 5.9. The distribution of the mass values obtained for $Z_c(3900)^-$ particle reconstructed from μ^+ and μ^- after the Mass Constraint Fit: Gauss Fit, Breit-Wigner Fit and Voigt Fit from left to right, respectively.

According to the first graphic in Figure 5.9, the red line represents the Gauss Fit distribution applied to the $Z_c(3900)^-$ particle candidates reconstructed in the range of 2.5-3.5 GeV/c^2. The mass value is 3.886 GeV and the width value is 0.134138 GeV after applying Gaussian Fit to $Z_c(3900)^-$ particle. These mass and width values are known as 3.888 GeV and 0.0283 GeV in the literature, respectively. When mass values are compared, the value in the literature is 99.94%

with an error rate of 0.051%. According to the secand graphic, the pink line represents the Breit-Wigner Fit Fit distribution applied to the $Z_c(3900)^-$ particle candidates reconstructed in the range of 3.5-4.5 GeV/c^2. The mass value is 3.888 GeV and the width value is 0.114 GeV after applying a Breit-Wigner Fit to $Z_c(3900)^-$ particle. When these results in the distribution are compared, the mass value is the same as in the PDG value. According to the third graphic, the green line represents the Voigt Fit distribution applied to the $Z_c(3900)^-$ particle candidates reconstructed in the range of 3.5-4.5 GeV/c^2. The mass value is 3.886 GeV and the width value is 0.05781 GeV after applying a Voigt Fit to $Z_c(3900)^-$ particle. When mass values are compared, the value in the literature is 99.94% with an error rate of 0.051%. 498268 events out of 1 Million have reconstructed $Z_c(3900)^-$ particle in this range which leads to the efficiency rate of 49.8%.

In order to obtain kinematic functions of $Z_c(3900)^-$ particle, three different distribution has been applied. First of all, Pt distribution is applied to the reconstructed mass distribution of μ^+ and μ^- system after Mass Constraint Fit. After the P_T distribution, the Eta distribution from the kinematic functions of the $Z_c(3900)^-$ particle is applied. The final kinematic function of $Z_c(3900)^-$particle is applied to the Phi distribution.

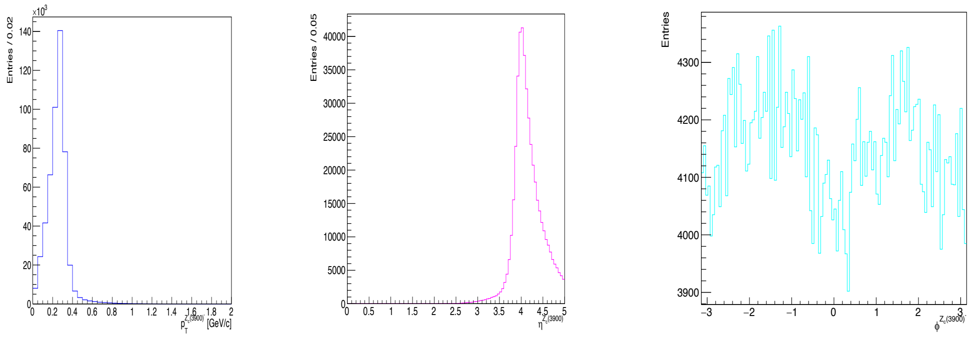

Figure 5.10. The distribution of kinematic variables of $Zc(3900)^-$ particle reconstructed from μ^+ and μ^- after the Mass Constraint Fit: $P_T^{Zc(3900)^-}$ (Transverse momentum) distribution, $\eta^{Zc(3900)^-}$ (Eta) distribution and $\phi^{Zc(3900)^-}$ (Phi) distribution from left to right, respectively.

Three different distributions are applied to obtain the kinematic values of the $Z_c(3900)^-$ particle. In the graph on the left, the Transverse momentum distribution of $Z_c(3900)^-$particle with a peak of 0.24 GeV/c in the range of 0 - 2 GeV/c is obtained. In the middle graph, the Eta distribution of $Z_c(3900)^-$particle with a peak of 4.14 in the range of 0-5 is obtained. In the right graph, the Phi distribution of $Z_c(3900)^-$ particle with a peak of 0.00018 in the range of -3 and 3 is obtained. 498268 events out of 1 Million have reconstructed of $Z_c(3900)^{--}$particle on P_T, Eta, Phi distribution which leads to the efficiency rate of 49.8%.

5.2.2 e^+e^- Channel

The $Z_c(3900)^-$ particle candidates are reconstructed by combining the e^+ and e^- candidates. The invariant mass distributions and kinematic valuable of the reconstructed $Z_c(3900)^-$particle candidates are observed.

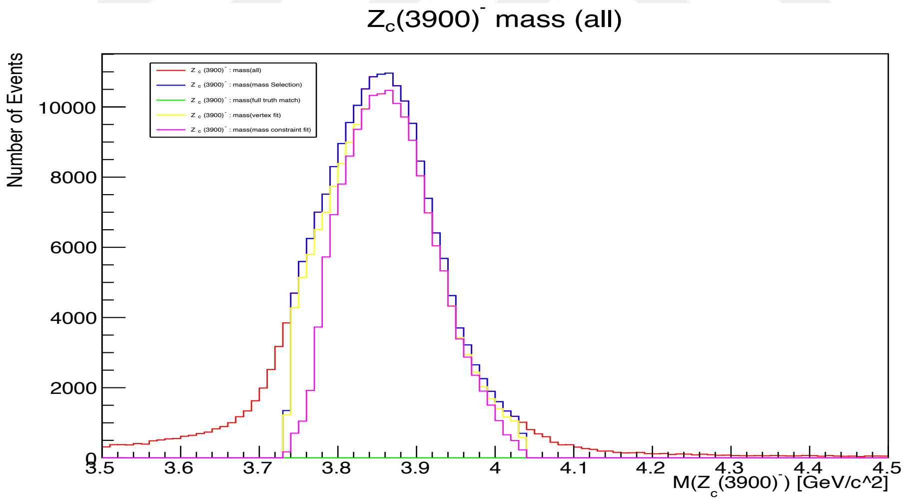

Figure 5.11. The invariant mass distributions of the $Z_c(3900)^-$ particle candidates reconstructed by e^+ and e^- after aplying different selection creteria.

In Figure 5.11, the invariant mass distributions of the $Z_c(3900)^-$particle candidates reconstructed by $e^+$and e^- is plotted in the range of 3.5-4.5 GeV/c^2 for different selection creteria to see the efect of it. Red line representes the events where all combinations of $e^+$and e^-combined to reconstruct $Z_c(3900)^-$ particle in the given range. 236191 events out of 1 Million have reconstructed $Z_c(3900)^-$ particle in this range which leads to the efficiency rate of 23.6%. Blue line represents the $Z_c(3900)^-$particle candidates after the Mass Selection cut which is $\pm$ 0.15 GeV/c^2 around the mass of $Z_c(3900)^-$ particle 3.886 GeV/c^2 reported in PDG. 193969 events out of 1 Million have reconstructed $Z_c(3900)^-$ particle in this range which leads to the efficiency rate of 19.3%. The green line represents the $Z_c(3900)^-$ particle candidates after the McTruthMatch algorithm was applied. 191643 events out of 1 Million have reconstructed $Z_c(3900)^-$ particle in this range which leads to the efficiency rate of 19.1%. The yellow line represents the $Z_c(3900)^-$ particle candidates after the Vertex Fit algorithm was applied with more than 1% probability. 182048 events out of 1Milyon have reconstructed $Z_c(3900)^-$ particle in this range which leads to the efficiency rate of 18.2%. The pink line represents a large reduction in the number of $Z_c(3900)^-$ particle candidates after Mass Constraint matching. 161177 events out of 1 Million have reconstructed $Z_c(3900)^-$ particle in this range which leads to the efficiency rate of 16.1%.

As can be seen in Figure 5.11, the invariant mass distributions of each particle in the decay chain are gradually restricted after each cut. It is seen that the peak in the desired mass range is sharpened and this peak approaches the mass of the $Z_c(3900)^-$ particle to be reconstructed.

In order to obtain mass and width of $Z_c(3900)^-$ particle, three different fit function has been applied. First of all, Gauss Fit is applied to the reconstructed mass distribution of e^+ and e^- system after Mass Constraint Fit. Mass and width are obtained for mass and width of $Z_c(3900)^-$ particle, respectively. When Breit-Wigner Fit is performed to the same distribution, mass and width are obtained. Finally, Voigt Fit gives better than other fits.

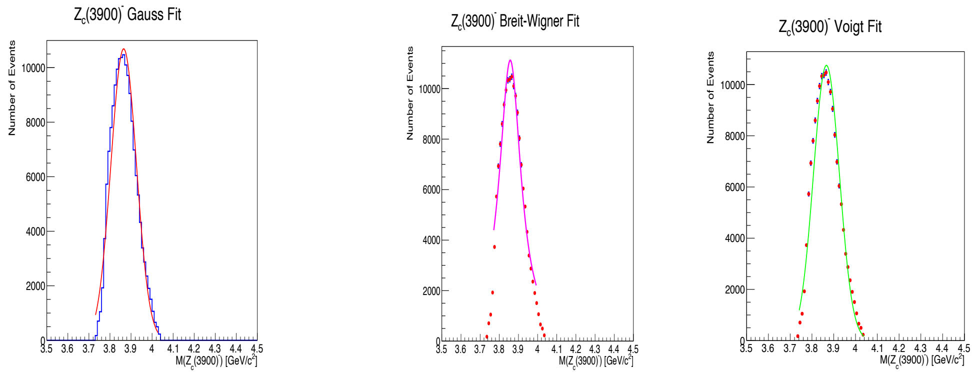

Figure 5.12. The distribution of the mass values obtained for $Z_c(3900)^-$ particle reconstructed from e^+ and e^- after the Mass Constraint Fit: Gauss Fit, Breit-Wigner Fit and Voigt Fit from left to right, respectively.

According to the first graphic in Figure 5.12, the red line represents the Gauss Fit distribution applied to the $Z_c(3900)^-$ particle candidates reconstructed in the range of 2.5-3.5 GeV/c^2. The mass value is 3.865 GeV and the width value is 0.142175 GeV after applying Gaussian Fit to $Z_c(3900)^-$ particle. These mass and width values are known as 3.888 GeV and 0.0283 GeV in the literature, respectively. When mass values are compared, the value in the literature is 99.40% with an error rate of 0.059%. According to the second graphic, the pink line represents the Breit-Wigner Fit Fit distribution applied to the $Z_c(3900)^-$ particle candidates reconstructed in the range of 3.5-4.5 GeV/c^2. The mass value is 3.86 GeV and the width value is 0.1376 GeV after applying a Breit-Wigner Fit to $Z_c(3900)^-$ particle. When mass values are compared, the value in the literature is 99.27% with an error rate of 0.72%. According to the third graphic, the green line represents the Voigt Fit distribution applied to the $Z_c(3900)^-$particle candidates reconstructed in the range of 3.5-4.5 GeV/c^2. The mass value is 3.886 GeV and the width value is 0.05947 GeV after applying a Voigt Fit to $Z_c(3900)^-$ particle. When mass values are compared, the value in the literature is 99.94 % with an error rate of 0.56%. 161177 events out of 1 Million have reconstructed $Z_c(3900)^-$ particle in this range which leads to the efficiency rate of 16.1%.

In order to obtain kinematic functions of $Z_c(3900)^-$ particle, three different distribution has been applied. First of all, Pt distribution is applied to the reconstructed mass distribution of e^+ and e^- system after Mass Constraint Fit. After the P_T distribution, the Eta distribution from the kinematic functions of the $Z_c(3900)^-$ particle is applied. The final kinematic function of $Z_c(3900)^-$particle is applied to the Phi distribution.

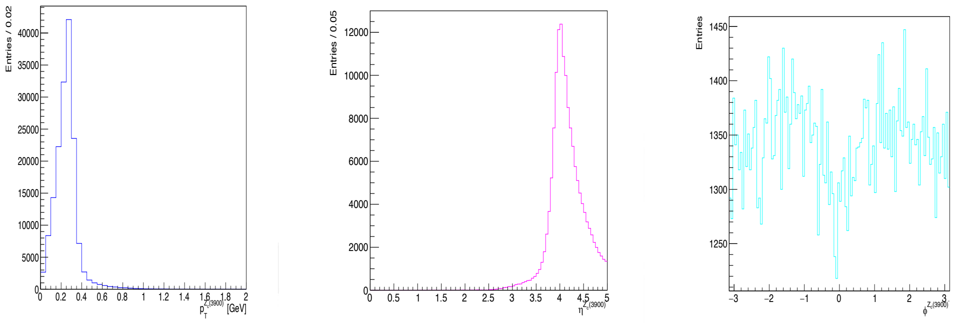

Figure 5.13. The distribution of kinematic variables of $Zc(3900)^-$ particle reconstructed from e^+ and e^- after the Mass Constraint Fit: $P_T^{Zc(3900)^-}$ (Transverse momentum) distribution,$\eta^{Zc(3900)^-}$(Eta) distribution and $\phi^{Zc(3900)^-}$(Phi) distribution from left to right, respectively.

Three different distributions are applied to obtain the kinematic values of the $Zc(3900)^-$ particle. In the graph on the left, the Transverse momentum distribution of $Zc(3900)^-$particle with a peak of 0.25 GeV/c in the range of 0 - 2 GeV/c is obtained. In the middle graph, the Eta distribution of $Zc(3900)^-$particle with a peak of 4.138 in the range of 0-5 is obtained. In the right graph, the Phi distribution of $Zc(3900)^-$ particle with a peak of 0.00115 in the range of -3 and 3 is obtained. 161177 events out of 1 Milyon have reconstructed of $Zc(3900)^-$particle on P_T, Eta, Phi distribution which leads to the efficiency rate of 16.1%.

5.3 Reconstruction of $\psi(4260)$ Particle

Not only the effects of different selection criteria but also Gauss Fit, Breit-Wigner Fit and Voigt Fit results to the distribution of invariant mass of μ^+, μ^- or e^+, e^- are discussed. Distribution of Kinematic variables for the reconstructed $\psi(4260)$ particle is also presented.

5.3.1 $\mu^+\mu^-$ Channel

The $\psi(4260)$ particle candidates are reconstructed by combining the μ^+ and μ^- candidates. The invariant mass distributions and kinematic valuable of the reconstructed $\psi(4260)$ particle candidates are observed.

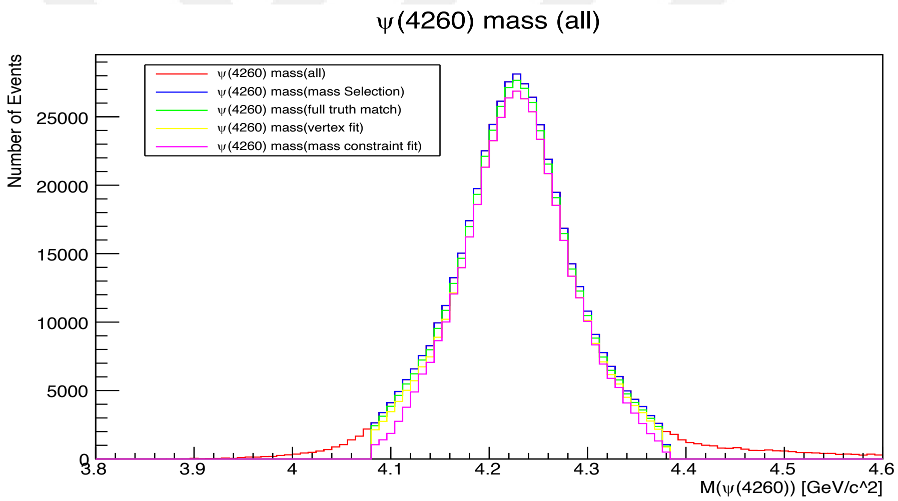

Figure 5.14. The invariant mass distributions of the $\psi(4260)$ particle candidates reconstructed by μ^+ and μ^- after aplying different selection creteria.

In Figure 5.14, the invariant mass distributions of the $\psi(4260)$ particle candidates reconstructed by μ^+ and μ^- is plotted in the range of 3.8-4.6 GeV/c^2 for different selection creteria to see the efect of it. Red line representes the events where all combinations of μ^+ and μ^- combined to reconstruct $\psi(4260)$ particle in the given range. 529632 events out of 1 Million have reconstructed $\psi(4260)$ particle in this range which leads to the efficiency rate of

52.9%. Blue line represents the $\psi(4260)$ particle candidates after the Mass Selection cut which is $\pm$ 0.15 GeV/c^2 around the mass of $\psi(4260)$ particle 3.886 GeV/c^2 reported in PDG. 482449 events out of 1 Million have reconstructed $\psi(4260)$ particle in this range which leads to the efficiency rate of 48.2%. The green line represents the $\psi(4260)$ particle candidates after the McTruthMatch algorithm was applied. 469959 events out of 1 Million have reconstructed $\psi(4260)$ particle in this range which leads to the efficiency rate of 46.9%.The yellow line represents the $\psi(4260)$ particle candidates after the Vertex Fit algorithm was applied with more than 1% probability. 450736 events out of 1 Million have reconstructed $\psi(4260)$ particle in this range which leads to the efficiency rate of 45%. The pink line represents a large reduction in the number of $\psi(4260)$ particle candidates after Mass Constraint matching. 436944 events out of 1 Million have reconstructed $\psi(4260)$ particle in this range which leads to the efficiency rate of 43.6%.

As can be seen in Figure 5.14, the invariant mass distributions of each particle in the decay chain are gradually restricted after each cut. It is seen that the peak in the desired mass range is sharpened and this peak approaches the mass of the $\psi(4260)$ particle to be reconstructed.

In order to obtain mass and width of $\psi(4260)$ particle, three different fit function has been applied. First of all, Gauss Fit is applied to the reconstructed mass distribution of μ^+ and μ^- system after Mass Constraint Fit. Mass and width are obtained for mass and width of $\psi(4260)$ particle, respectively. When Breit-Wigner Fit is performed to the same distribution, mass and width are obtained. Finally, Voigt Fit gives better than other fits.

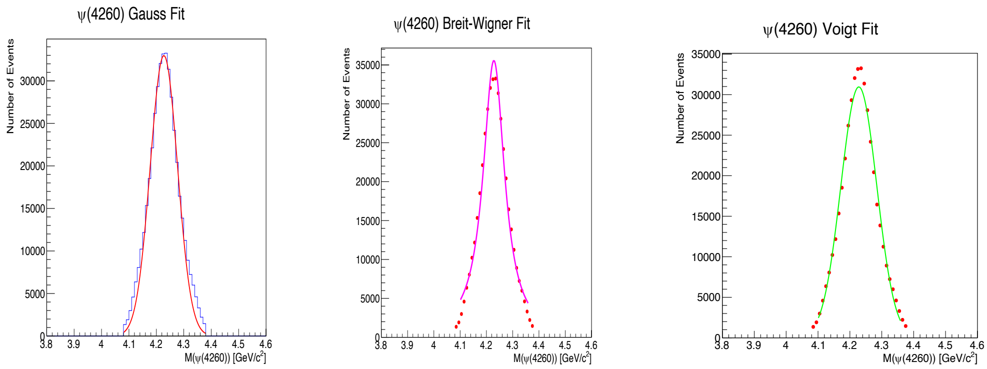

Figure 5.15. The distribution of the mass values obtained for $\psi(4260)$ particle reconstructed from μ^+ and μ^- after the Mass Constraint Fit: Gauss Fit, Breit-Wigner Fit and Voigt Fit from left to right, respectively.

According to the first graphic in Figure 5.15, the red line represents the Gauss Fit distribution applied to the $\psi(4260)$ particle candidates reconstructed in the range of 3.8- 4.6 GeV/c^2. The mass value is 4.227 GeV and the width value is 0.116 GeV after applying Gaussian Fit to $\psi(4260)$ particle. These mass and width values are known as 4.230 GeV and 0.055 GeV in the literature, respectively. When mass values are compared, the value in the literature is 99.92% with an error rate of 0.070%. According to the second graphic, the pink line represents the Breit-Wigner Fit Fit distribution applied to the $\psi(4260)$ particle candidates reconstructed in the range of 3.8-4.6 GeV/c^2. The mass value is 4.23 GeV and the width value is 0.09934 GeV after applying a Breit-Wigner Fit to$\psi(4260)$ particle. When these results in the distribution are compared, the mass value is the same as in the PDG value. According to the third graphic, the green line represents the Voigt Fit distribution applied to the $\psi(4260)$ particle candidates reconstructed in the range of 3.8-4.6 GeV/c^2. The mass value is 4.228 GeV and the width value is 0.0563 GeV after applying a Voigt Fit to $\psi(4260)$ particle. When mass values are compared, the value in the literature is 99.96 % with an error rate of 0.047%. 436944 events out of 1 Million have reconstructed $\psi(4260)$ particle in this range which leads to the efficiency rate of 43.6%.

In order to obtain kinematic functions of $\psi(4260)$ particle, three different distribution has been applied. First of all, P_T distribution is applied to the reconstructed mass distribution of μ^+ and μ^- system after Mass Constraint Fit. After the P_T distribution, the Eta distribution from the kinematic functions of the $\psi(4260)$ particle is applied. The final kinematic function of $\psi(4260)$ particle is applied to the Phi distribution.

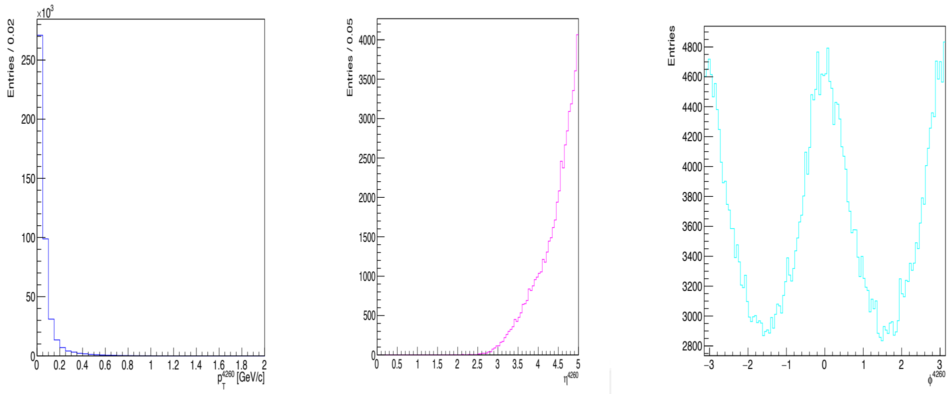

Figure 5.16. The distribution of kinematic variables of $\psi(4260)$ particle reconstructed from μ^+ and μ^- after the Mass Constraint Fit: $P_T^{\psi(4260)}$ (Transverse momentum) distribution, $\eta^{\psi(4260)}$ Eta distribution and $\phi^{\psi(4260)}$ (Phi distribution from left to right, respectively.

Three different distributions are applied to obtain the kinematic values of the $\psi(4260)$ particle. In the graph on the left, the Transverse momentum distribution of $\psi(4260)$ particle with a peak of 0.065 GeV/c in the range of 0-2 GeV/c is obtained. In the middle graph, the Eta distribution of $\psi(4260)$ particle with a peak of 4.42 in the range of 0-5 is obtained. In the right graph, the Phi distribution of $\psi(4260)$ particle with a peak of 0.0007126 in the range of -3 and 3 is obtained. 436944 events out of 1 Million have reconstructed of $\psi(4260)$ particle on P_T, Eta, Phi distribution which leads to the efficiency rate of 43.6%.

5.3.2 e^+e^- Channel

The $\psi(4260)$ particle candidates are reconstructed by combining the e^+ and e^- candidates. The invariant mass distributions and kinematic valuable of the reconstructed $\psi(4260)$ particle candidates are observed.

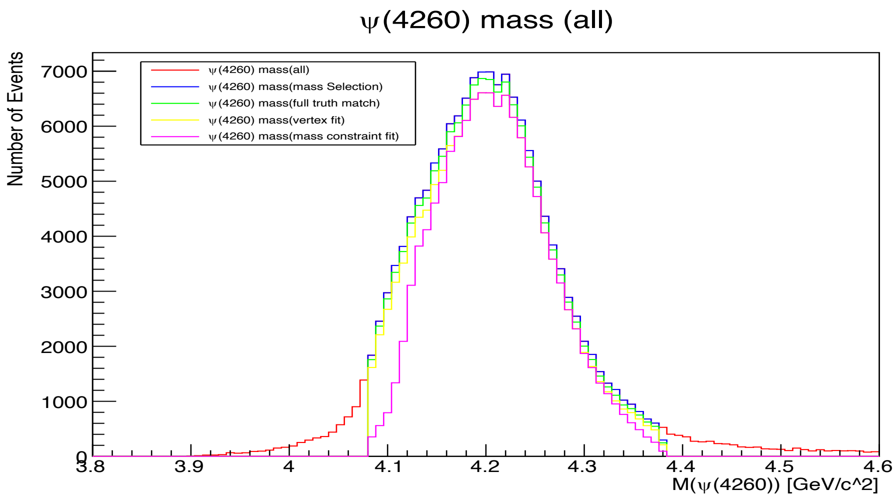

Figure 5.17. The invariant mass distributions of the $\psi(4260)$ particle candidates reconstructed by e^+ and e^- after aplying different selection creteria.

In Figure 5.17, the invariant mass distributions of the $\psi(4260)$ particle candidates reconstructed by e^+ and e^- is plotted in the range of 3.8-4.6 GeV/c^2 for different selection creteria to see the efect of it. Red line representes the events where all combinations of e^+ and e^- combined to reconstruct $\psi(4260)$ particle in the given range. 161688 events out of 1 Million have reconstructed $\psi(4260)$ particle in this range which leads to the efficiency rate of 16.1%. Blue line represents the $\psi(4260)$ particle candidates after the Mass Selection cut which is $\pm$ 0.15 GeV/c^2 around the mass of $\psi(4260)$ particle 4.230 GeV/c^2 reported in PDG. 145299 events out of 1 Million have reconstructed $\psi(4260)$ particle in this range which leads to the efficiency rate of 14.5%. The green line represents the $\psi(4260)$ particle candidates after the McTruthMatch algorithm was applied. 141250 events out of 1 Million have reconstructed $\psi(4260)$ particle in this range which leads to the efficiency rate of 14.1%. The yellow line represents the $\psi(4260)$ particle candidates after the Vertex Fit algorithm was applied with more than 1% probability. 134685 events out of 1 Million have reconstructed $\psi(4260)$ particle in this range which leads to the efficiency rate of 13.4%. The pink line represents a large reduction in the number of $\psi(4260)$ particle candidates after Mass Constraint matching. 123027 events out of 1 Million have reconstructed $\psi(4260)$ particle in this range which leads to the efficiency rate of 12.3%.

As can be seen in Figure 5.17, the invariant mass distributions of each particle in the decay chain are gradually restricted after each cut. It is seen that the peak in the desired mass range is sharpened and this peak approaches the mass of the $\psi(4260)$ particle to be reconstructed.

In order to obtain mass and width of $\psi(4260)$ particle, three different fit function has been applied. First of all, Gauss Fit is applied to the reconstructed mass distribution of e^+ and e^- system after Mass Constraint Fit. Mass and width are obtained for mass and width of $\psi(4260)$ particle, respectively. When Breit-Wigner Fit is performed to the same distribution, mass and width are obtained. Finally, Voigt Fit gives better than other fits.

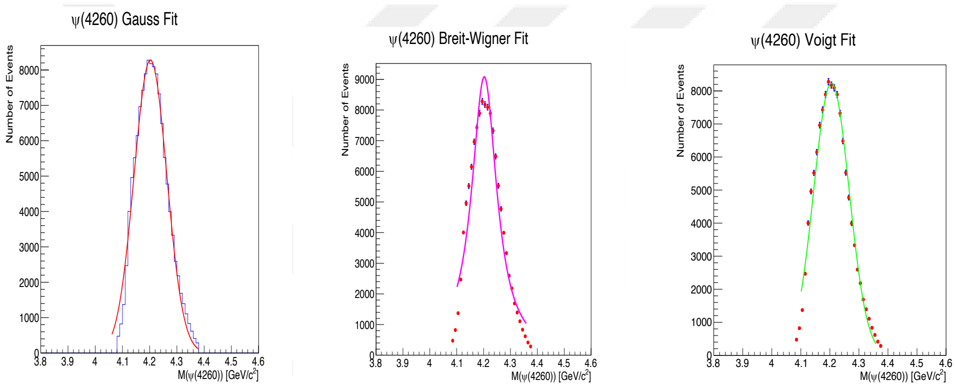

Figure 5.18. The distribution of the mass values obtained for $\psi(4260)$ particle reconstructed from e^+ and e^- after the Mass Constraint Fit: Gauss Fit, Breit-Wigner Fit and Voigt Fit from left to right, respectively.

According to the first graphic in Figure 5.18, the red line represents the Gauss Fit distribution applied to the $\psi(4260)$ particle candidates reconstructed in the range of 3.8-4.6 GeV/c^2. The mass value is 4.203 GeV and the width value is 0.14147 GeV after applying Gaussian Fit to $\psi(4260)$ particle. These mass and width values are known as 4.230 GeV and 0.055 GeV in the literature, respectively. When mass values are compared, the value in the literature is 99.36% with an error rate of 0.63. According to the secand graphic, the pink line represents the Breit-Wigner Fit Fit distribution applied to the$\psi(4260)$ particle candidates reconstructed in the range of 3.8-4.6 GeV/c^2. The mass value is 4.204 GeV and the width value is 0.1142 GeV after applying a Breit-Wigner Fit to$\psi(4260)$ particle. When mass values are compared, the value in the literature is 99.38 % with an error rate of 0.61%. According to the third graphic, the green line represents the Voigt Fit distribution applied to the $\psi(4260)$ particle candidates reconstructed in the range of 3.8-4.6 GeV/c^2. The mass value is 4.205 GeV and the width value is 0.06103 GeV after applying Voigt Fit to $\psi(4260)$ particle. When mass values are compared, the value in the literature is 99.40% with an error rate of 0.59%. 123027 events out of 1 Million have reconstructed $\psi(4260)$ particle in this range which leads to the efficiency rate of 12.3%.

In order to obtain kinematic functions of $\psi(4260)$ particle, three different distribution has been applied. First of all, P_T distribution is applied to the reconstructed mass distribution of e^+ and e^- system after Mass Constraint Fit. After the P_T distribution, the Eta distribution from the kinematic functions of the $\psi(4260)$ particle is applied. The final kinematic function of $\psi(4260)$ particle is applied to the Phi distribution.

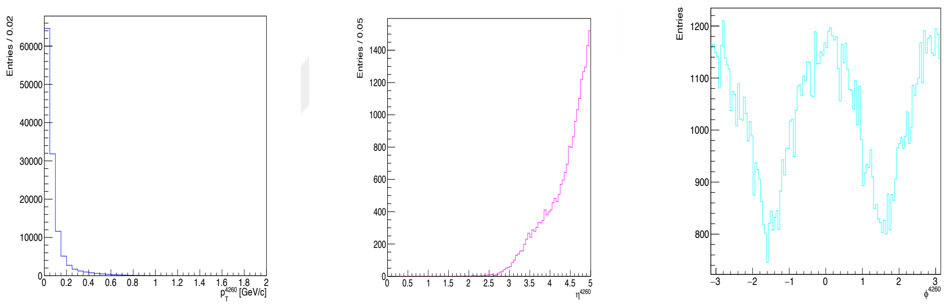

Figure 5.19. The distribution of kinematic variables of $\psi(4260)$ particle reconstructed from e^+ and e^- after the Mass Constraint Fit: $P_T^{\psi(4260)}$ (Transverse momentum) distribution, $\eta^{\psi(4260)}$ (Eta) distribution and $\phi^{\psi(4260)}$ (Phi) distribution from left to right, respectively.

Three different distributions are applied to obtain the kinematic values of the $\psi(4260)$ particle. In the graph on the left, the Transverse momentum distribution of $\psi(4260)$ particle with a peak of 0.08 GeV/c in the range of 0-2 GeV/c is obtained. In the middle graph, the Eta distribution of $\psi(4260)$ particle with a peak of 4.37 in the range of 0-5 is obtained. In the right graph, the Phi distribution of $\psi(4260)$ particle with a peak of 0.08051 in the range of -3 and 3 is obtained. 123027 events out of 1 Million have reconstructed of $\psi(4260)$ particle on P_T, Eta, Phi distribution which leads to the efficiency rate of 12.3%.

5.4 Reconstruction of J/ψ Daughter Particle

Not only the effects of different selection criteria but also Gauss Fit, Breit-Wigner Fit and Voigt Fit results to the distribution of invariant mass of μ^+, μ^- or e^+, e^- are discussed. Distribution of Kinematic variables for the reconstructed J/ψ daughter particles are also presented.

5.4.1 $\mu^+\mu^-$ Channel

In order to obtain mass and width of daughter particle, three different fit function has been applied. First of all, Gauss Fit is applied to the reconstructed mass distribution of μ^+ and μ^- system after Mass Constraint Fit. Mass and width are obtained for mass and width of J/ψ daughter respectively. When Breit-Wigner Fit is performed to the same distribution, mass and width are obtained. Finally, Voigt Fit gives better than other fits.

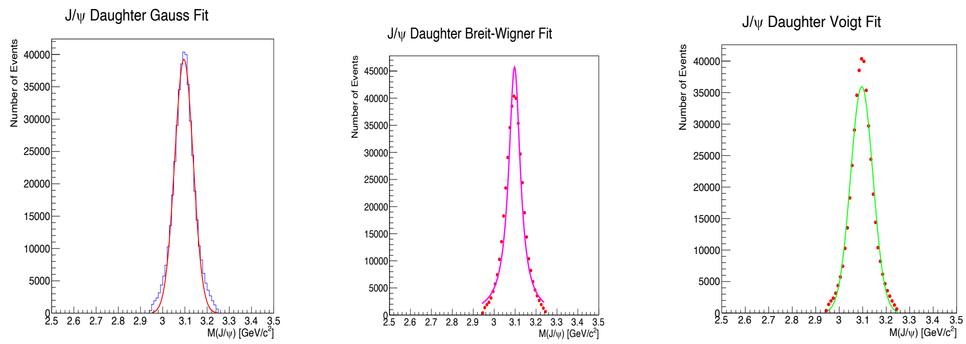

Figure 5.20. The distribution of the mass values obtained J/ψ daughter particle reconstructed from $\mu^+$and μ^- after the Mass Constraint Fit: Gauss Fit, Breit-Wigner Fit and Voigt Fit from left to right, respectively.

According to the first graphic in Figure 5.20, the red line represents the Gauss Fit distribution applied to the J/ψ daughter particle candidates reconstructed in the range of 2.5-3.5 GeV/c^2. The mass value is 3.096 GeV and the width value is 0.097948 GeV after applying Gaussian Fit to J/ψ particle. These mass and width values are known as 3.096 GeV and 0.0000929 GeV in the literature, respectively. When these results in the distribution are compared, the mass value is the same as in the PDG value. According to the secand graphic, the pink line represents the Breit-Wigner Fit Fit distribution applied to the J/ψ daughter particle candidates reconstructed in the range of 2.5-3.5 GeV/c^2. The mass value is 3.098 GeV and the width value is 0.06722 GeV after applying a Breit-Wigner Fit to J/ψ daughter particle. When mass values are compared, the value in the literature is 99.93% with an error rate of 0.064%. According to the third graphic, the green line represents the Voigt Fit distribution applied to the J/ψ daughter particle candidates reconstructed in the range of 2.5-3.5 GeV/c^2. The mass value is 3.096 GeV and the width value is 0.04763 GeV after applying a Voigt Fit to J/ψ daughter particle. When these results in the distribution are compared, the mass value is the same as in the PDG value. 436944 events out of 1 Million have reconstructed J/ψ particle daughter in this range which leads to the efficiency rate of 43.6%.

5.4.2 e^+e^- Channel

In order to obtain mass and width of J/ψ daughter particle, three different fit function has been applied. First of all, Gauss Fit is applied to the reconstructed mass distribution of e^+ and e^- system after Mass Constraint Fit. Mass and width are obtained for mass and width of J/ψ daughter respectively. When Breit-Wigner Fit is performed to the same distribution, mass and width are obtained. Finally, Voigt Fit gives better than other fits.

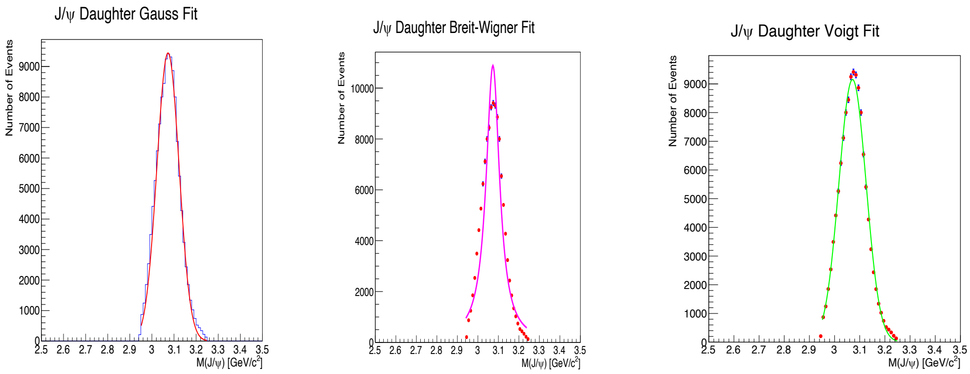

Figure 5.21. The distribution of the mass values obtained J/ψ daughter particle reconstructed from e^+ and e^- after the Mass Constraint Fit: Gauss Fit, Breit-Wigner Fit and Voigt Fit from left to right, respectively.

According to the first graphic in Figure 5.21, the red line represents the Gauss Fit distribution applied to the J/ψ daughter particle candidates reconstructed in the range of 2.5-3.5 GeV/c^2. The mass value is 3.073 GeV and the width value is 0.117829 GeV after applying Gaussian Fit to J/ψ daughter particle. These mass and width values are known as 3.096 GeV and 0.0000929 GeV in the literature, respectively. When mass values are compared, the value in the literature is 99.25% with an error rate of 0.74%. According to the second graphic, the pink line represents the Breit-Wigner Fit Fit distribution applied to the J/ψ daughter particle candidates reconstructed in the range of 2.5-3.5 GeV/c^2. The mass value is 3.074 GeV and the width value is 0.07997 GeV after applying a Breit-Wigner Fit to J/ψ daughter particle. When mass values are compared, the value in the literature is 99.28% with an error rate of 0.71%. According to the third graphic, the green line represents the Voigt Fit distribution applied to the J/ψ daughter particle candidates reconstructed in the range of 2.5-3.5 GeV/c^2. The mass value is 3.071 GeV and the width value is 0.05396 GeV after applying a Voigt Fit to J/ψ daughter particle. When mass values are compared, the value in the literature is 99.19% with an error rate of 0.80%. 123027 events out of 1 Million have reconstructed J/ψ daughter particle in this range which leads to the efficiency rate of 12.3%.

5.5 Reconstruction of $Z_c(3900)^-$ Daughter Particle

Not only the effects of different selection criteria but also Gauss Fit, Breit-Wigner Fit and Voigt Fit results to the distribution of invariant mass of μ^+, μ^- or e^+, e^- are discussed. Distribution of Kinematic variables for the reconstructed $Z_c(3900)^-$daughter particles are also presented.

5.5.1 $\mu^+\mu^-$ Channel

In order to obtain mass and width of $Z_c(3900)^-$ daughter particle, three different fit function has been applied. First of all, Gauss Fit is applied to the reconstructed mass distribution of μ^+ and μ^- system after Mass Constraint Fit. Mass and width are obtained for mass and width of J/ψ daughter respectively. When Breit-Wigner Fit is performed to the same distribution, mass and width are obtained. Finally, Voigt Fit gives better than other fits.

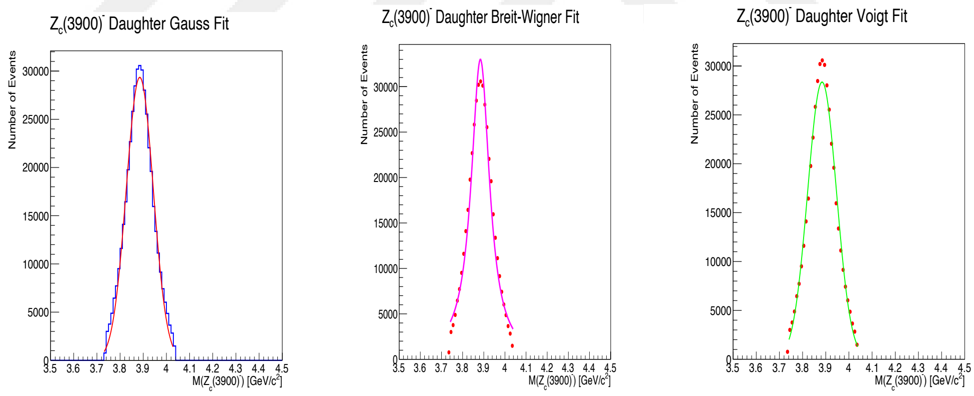

Figure 5.22. The distribution of the mass values obtained $Z_c(3900)^-$ daughter particle reconstructed from μ^+ and μ^- after the Mass Constraint Fit: Gauss Fit, Breit-Wigner Fit and Voigt Fit from left to right, respectively.

According to the first graphic in Figure 5.22, the red line represents the Gauss Fit distribution applied to the $Z_c(3900)^-$ daughter particle candidates reconstructed in the range of 3.5-4.5 GeV/c^2. The mass value is 3.885 GeV and the width value is 0.13679 GeV after applying Gaussian Fit to $Z_c(3900)^-$ daughter particle. These mass and width values are known as 3.888 GeV and 0.0283 GeV in the literature, respectively. When mass values are compared, the value in the literature is 99.92% with an error rate of 0.077%. According to the secand graphic, the pink line represents the Breit-Wigner Fit Fit distribution applied to the J/ψ particle candidates reconstructed in the range of 3.5-4.5 GeV/c^2. The mass value is 3.885 GeV and the width value is 0.1057 GeV after applying a Breit-Wigner Fit to $Z_c(3900)^-$daughter particle. When mass values are compared, the value in the literature is 99.92% with an error rate of 0.077%. According to the third graphic, the green line represents the Voigt Fit distribution applied to the $Z_c(3900)^-$ daughter particle candidates reconstructed in the range of 3.5-4.5 GeV/c^2. The mass value is 3.884 GeV and the width value is 0.06205 GeV after applying a Voigt Fit to $Z_c(3900)^-$ daughter particle. When mass values are compared, the value in the literature is 99.89% with an error rate of 0.10%. 436944 events out of 1 Million have reconstructed $Z_c(3900)^-$ daughter particle in this range which leads to the efficiency rate of 43.6%.

5.5.2 e^+e^- Channel

In order to obtain mass and width of $Z_c(3900)^-$ daughter particle, three different fit function has been applied. First of all, Gauss Fit is applied to the reconstructed mass distribution of e^+ and e^- system after Mass Constraint Fit. Mass and width are obtained for mass and width of J/ψ daughter respectively. When Breit-Wigner Fit is performed to the same distribution, mass and width are obtained. Finally, Voigt Fit gives better than other fits.

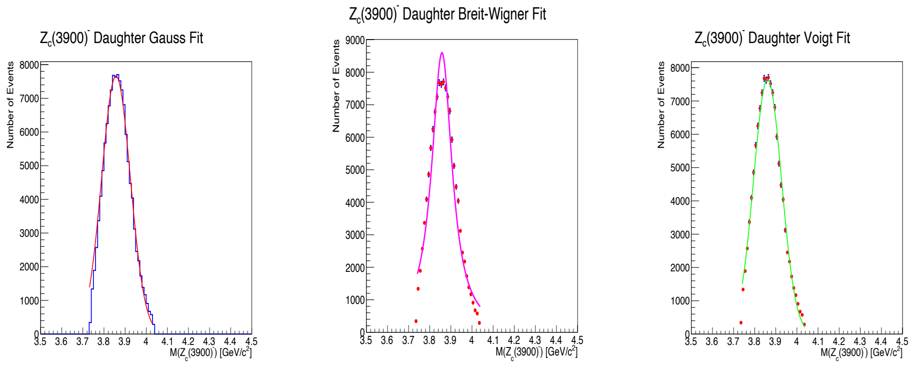

Figure 5.23. The distribution of the mass values obtained $Z_c(3900)^-$ daughter particle reconstructed from e^+ and e^- after the Mass Constraint Fit: Gauss Fit, Breit-Wigner Fit and Voigt Fit from left to right, respectively.

According to the first graphic in Figure 5.23, the red line represents the Gauss Fit distribution applied to the $Z_c(3900)^-$ daughter particle candidates reconstructed in the range of 3.5-4.5 GeV/c^2. The mass value is 3.857 GeV and the width value is 0.09588 GeV after applying Gaussian Fit to $Z_c(3900)^-$daughter particle. These mass and width values are known as 3.888 GeV and 0.0283 GeV in the literature, respectively. When mass values are compared, the value in the literature is 99.20% with an error rate of 0.79%. According to the secand graphic, the pink line represents the Breit-Wigner Fit Fit distribution applied to the $Z_c(3900)^-$ daughter particle candidates reconstructed in the range of 3.5-4.5 GeV/c^2. The mass value is 3.860 GeV and the width value is 0.1178 GeV after applying a Breit-Wigner Fit to $Z_c(3900)^-$daughter particle. When mass values are compared, the value in the literature is 99.27% with an error rate of 0.72%. According to the third graphic, the green line represents the Voigt Fit distribution applied to the $Z_c(3900)^-$ daughter particle candidates reconstructed in the range of 3.5-4.5 GeV/c^2. The mass value is 3.861 GeV and the width value is 0.06625 GeV after applying a Voigt Fit to $Z_c(3900)^-$ daughter particle. When mass values are compared, the value in the literature is 99.30% with an error rate of 0.69%. 123027 events out of 1 Million have reconstructed $Z_c(3900)^-$ daughter particle in this range which leads to the efficiency rate of 12.3%.

6. CONCLUSIONS AND RECOMMENDATIONS

In this thesis, the feasibility study of the exotic $Z_c(3900)^-$ particle for PANDA experiment was conducted. Simulation, data production and analysis studies of $Z_c(3900)^-$ particles were performed with PandaRoot Software. During the analysis, various fit algorithms were applied to the invariant mass distribution of $Z_c(3900)^-$ particle. The mass and width values of the applied cut and fit distributions were compared with the values in PDG.

The mass and width values of J/ψ, $Z_c(3900)^-$ and $\psi(4260)$ particles obtained from the Gauss Fit, Breit-Wigner Fit and Voigt Fit on the invariant mass distributions are shown in Figure 6.1, Figure 6.2, Figure 6.3 and Figure 6.4. In the Figure 6.1, the obtained mass values after the Gauss Fit, Breit-Wigner Fit and Voigt Fit to the invariant mass distributions for J/ψ particle reconstructed from for μ^+, μ^- are indicated with a red triangle. In this graph, the current mass value of J/ψ particle reported in PDG is indicated as a black triangle. The mass values 3.095 GeV, 3.097 GeV and 3.096 GeV are obtined from Gauss Fit, Breit-Wigner Fit and Voigt Fit, respectively. The mass value of J/ψ particle is known as 3.096 GeV in PDG. The graph shows that the mass value obtained with the Voigt Fit to invariant mass distribution of the reconstructed J/ψ particle is within the mass range defined by the PDG.

Results of the fits to the invariant mass distribution of $Z_c(3900)^-$ particle reconstructed from J/ψ and π^- is given in the middle plot of Figure 6.1. The blue square indicates the obtained mass results from the fits while black square is for PDG value. The mass values 3.886 GeV, 3.888 GeV and 3.886 GeV are obtined from Gauss Fit, Breit-Wigner Fit and Voigt Fit, respectively. The mass value of $Z_c(3900)^-$ particle is reported as 3.888 GeV in PDG. The graph shows that the mass value of the Breit-Wigner Fit distribution of the reconstructed $Z_c(3900)^-$ particle is within the mass range defined by the PDG.

Finally, results of $\psi(4260)$ mass values obtained with different fits are shown in the bottom plot of Figure 6.1. The green circle indicates the obtained mass results from the fits while black circle is for PDG value. The mass value obtained with the Gauss Fit is 4.227 GeV, the mass value obtained with the Breit-Wigner Fit is 4.23 GeV and the mass value obtained with the Voigt Fit is 4.230 GeV. The mass value of $\psi(4260)$ particle is known as 4.230 GeV in PDG. The graph shows that the mass value of the Breit-Wigner Fit distribution of the reconstructed $\psi(4260)$ particle is within the mass range defined by the PDG.

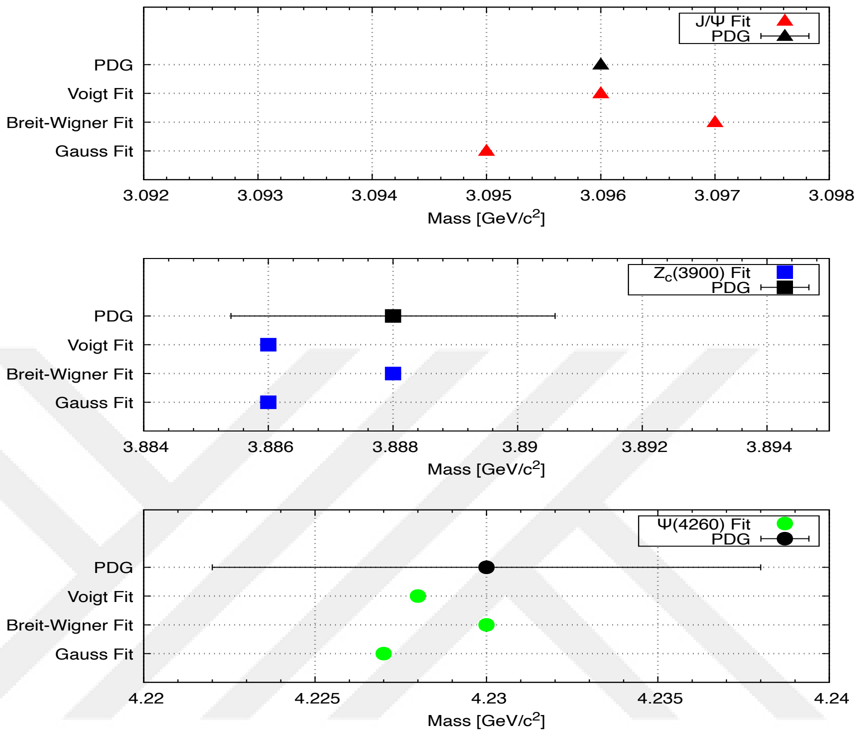

Figure 6.1. Comparison of the masses obtained from the Gauss Fit, Breit-Wigner Fit and Voigt Fit with PDG: J/ψ , $Z_c(3900)^-$ and $\psi(4260)$ particles (top to bottom) after all the cuts for μ^+, μ^- , π^+ and π^- final state.

In Figure 6.2, the obtained width values after the Gauss Fit, Breit-Wigner Fit and Voigt Fit to the distributions for J/ψ particle are indicated with a red triangle. In the graph, the width value of J/ψ particle reported in PDG is indicated as a black triangle. The width values 0.095888 GeV, 0.07902 GeV and 0.03492 GeV are obtined from Gauss Fit, Breit-Wigner Fit and Voigt Fit, respectively. The width value of J/ψ particle is known as 0.0000929 GeV in PDG. According to the result of the fit distributions of the J/ψ particle reconstructed in the graph, the width values are quite far from the values in PDG.

Results of the fits to the width distribution of $Z_c(3900)^-$ particle is given in the second graph of Figure 6.2. The blue square indicates the obtained width results from the fits while black square is for PDG value. The width values 0.134138 GeV, 0.114 GeV and 0.05781 GeV are obtined from Gauss Fit, Breit-Wigner Fit and Voigt Fit, respectively. The width value of $Z_c(3900)^-$ particle is reported as 0.0284 GeV in PDG. The graph shows that the width value of the Voigt Fit distribution of the reconstructed $Z_c(3900)^-$ particle approaches the width value defined by the PDG.

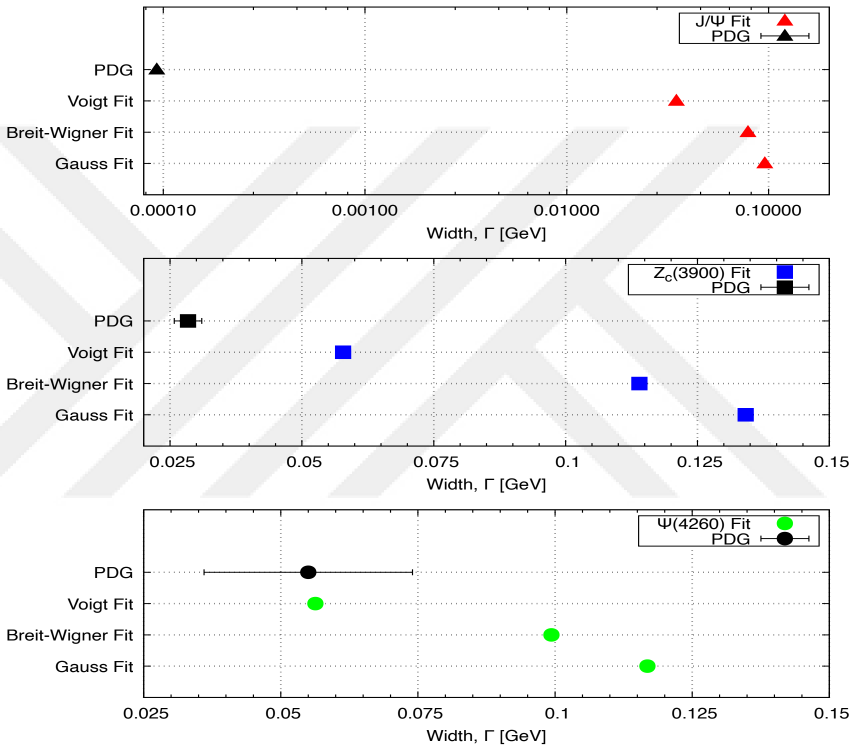

Figure 6.2. Comparison of the widthes obtained from the Gauss Fit, Breit-Wigner Fit and Voigt Fit width PDG: J/ψ , $Z_c(3900)^-$ and $\psi(4260)$ particles (top to bottom) after all the cuts for μ^+, μ^- , π^+ and π^- final state.

Finally, results of $\psi(4260)$ particle width values obtained with different fits are shown in the bottom plot of Figure 6.2. The green circle indicates the obtained mass results from the fits while black circle is for PDG value. The width value obtained with the Gauss Fit is 0.116842 GeV, the width value obtained with the Breit-Wigner Fit is 0.09934 GeV and the width value obtained with the Voigt Fit is 0.0563 GeV. The width value of $\psi(4260)$ particle is known as 0.055 GeV in

PDG. The graph shows that the width value of the Voigt Fit distribution of the reconstructed $\psi(4260)$ particle approaches the width value defined by the PDG.

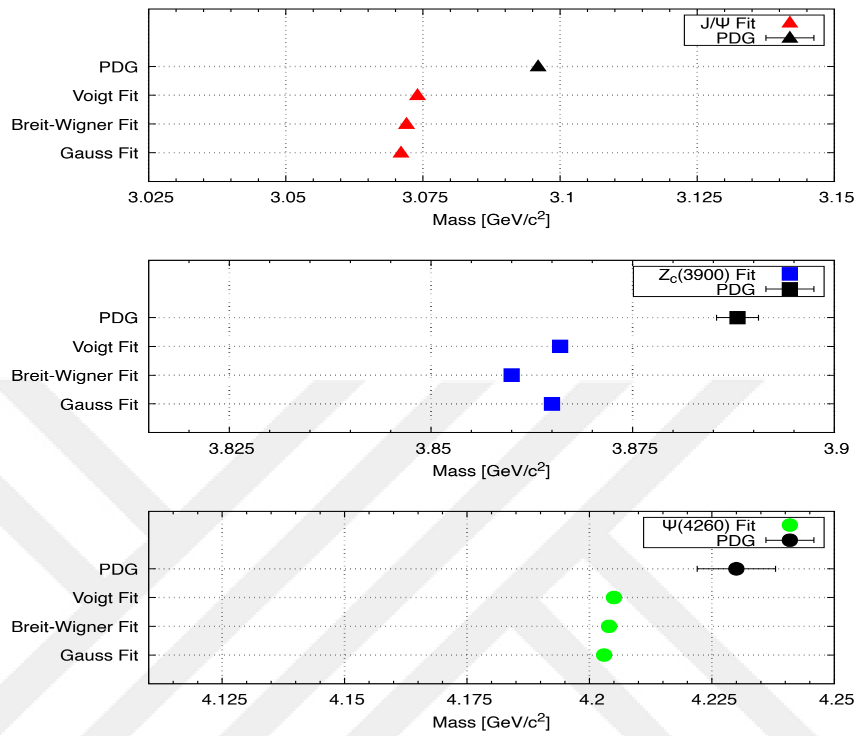

Figure 6.3. Comparison of the masses obtained from the Gauss Fit, Breit-Wigner Fit and Voigt Fit with PDG: J/ψ , $Z_c(3900)^-$ and $\psi(4260)$ particles (top to bottom) after all the cuts for e^+, e^- , π^+ and π^- final state.

In the top plot of Figure 6.3., the obtained mass values after the Gauss Fit, Breit-Wigner Fit and Voigt Fit to the invariant mass distributions for J/ψ particle reconstructed from for e^+, e^- are indicated with a red triangle. In the graph, the current mass value of J/ψ particle reported in PDG is indicated as a black triangle. The mass values 3.071 GeV, 3.072 GeV and 3.074 GeV are obtined from Gauss Fit, Breit-Wigner Fit and Voigt Fit, respectively. The mass value of J/ψ particle is known as 3.096 GeV in PDG. The graph shows that the mass distribution of the reconstructed J/ψ particle approximates the invariant mass value obtained by Voigt fit to the mass value defined by the PDG.

Results of the fits to the invariant mass distribution of $Z_c(3900)^-$ particle is given in the middle plot of Figure 6.3.The blue square indicates the obtained mass results from the fits while black square is for PDG value. The mass values 3.865 GeV, 3.86 GeV and 3.886 GeV are obtined from Gauss Fit, Breit-Wigner Fit and Voigt Fit, respectively. The mass value of $Z_c(3900)^-$ particle is reported as 3.888 GeV in PDG. The graph shows that the mass value of the Breit-Wigner Fit distribution of the reconstructed $Z_c(3900)^-$ particle is within the mass range defined by the PDG.

In the bottom plot of Figure 6.3., results of $\psi(4260)$ mass values obtained with different fits are shown in the bottom plot of Figure 6.3.The green circle indicates the obtained mass results from the fits while black circle is for PDG value. The mass value obtained with the Gauss Fit is 4.203 GeV, the mass value obtained with the Breit-Wigner Fit is 4.204 GeV and the mass value obtained with the Voigt Fit is 4.205 GeV. The mass value of $\psi(4260)$ particle is known as 4.230 GeV in PDG. The graph shows that the mass value of the Voigt Fit distribution of the reconstructed $\psi(4260)$ particle approaches the width value defined by the PDG.

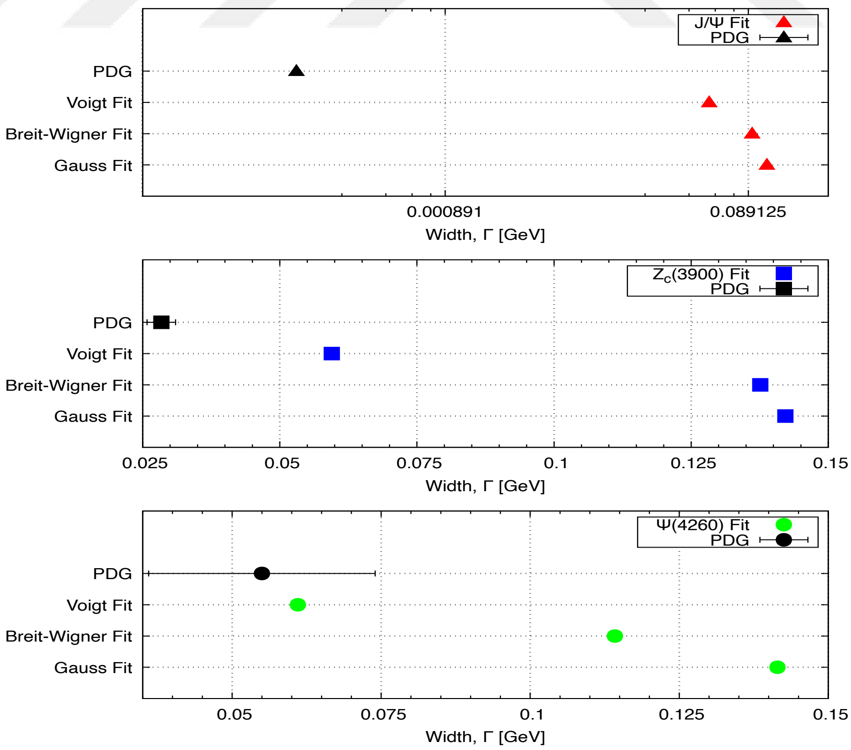

Figure 6.4. Comparison of the widthes obtained from the Gauss Fit, Breit-Wigner Fit and Voigt Fit width PDG: J/ψ , $Z_c(3900)^-$ and $\psi(4260)$ particles (top to bottom) after all the cuts for e^+, e^- , π^+ and π^- final state.

Firstly, the obtained mass values after the Gauss Fit, Breit-Wigner Fit and Voigt Fit to the invariant mass distributions for J/ψ particle are indicated with a red triangle. In the graph, the current mass value of J/ψ particle reported in PDG is indicated as a black triangle. The mass values 0.118158 GeV, 0.09437 GeV and 0.04914 GeV are obtined from Gauss Fit, Breit-Wigner Fit and Voigt Fit, respectively. The mass value of J/ψ particle is known as 0.0000929 GeV in PDG. According to the result of the fit distributions of the J/ψ particle reconstructed in the graph, the width values are quite far from the values in PDG.

Results of the fits to the width distribution of $Z_c(3900)^-$ particle is given in the middle plot of Figure 6.4.The blue square indicates the obtained mass results from the fits while black square is for PDG value. The width values 0.142175 GeV, 0.1376 GeV and 0.05947 GeV are obtined from Gauss Fit, Breit-Wigner Fit and Voigt Fit, respectively. The mass value of $Z_c(3900)^-$ particle is reported as 0.0284 GeV in PDG. The graph shows that the mass value of the Breit-Wigner Fit distribution of the reconstructed $Z_c(3900)^-$ particle approaches the width valued defined by the PDG.

In the last graph, results of $\psi(4260)$ width values obtained with different fits are shown in the bottom plot of Figure 6.4. The green circle indicates the obtained mass results from the fits while black circle is for PDG value. The width value obtained with the Gauss Fit is 0.14147 GeV, the width value obtained with the Breit-Wigner Fit is 0.1142 GeV and the width value obtained with the Voigt Fit is 0.06103 GeV. The width value of $\psi(4260)$ particle is known as 0.055 GeV in PDG. The graph shows that the width value of the Voigt Fit distribution of the reconstructed $\psi(4260)$ particle approaches the width value defined by the PDG.

To summarize, after applying different fit algorithms to the invariant mass distribution of reconstructed $Z_c(3900)^-$ particle, Voigt fit gave the best result, closest to the mass value in PDG. This can be seen from Figure 6.1, Figure 6.2, Figure 6.3 and Figure 6.4. Among the decay trees considered in this thesis (i.e. e^+, e^- , π^+ and π^- or μ^+, μ^- , π^+ and π^-), the efficiency obtained from the μ^+, μ^- channels are higher than that e^+, e- channels. The simulation of the PANDA dedector integrated into the PandaRoot Software has been successfully performed and feasibility studies of $Z_c(3900)^-$ particle have been conducted. These studies will contribute to the physics program is in the future.

7. REFERENCES

"Vancouver citiation system was used in this thesis."

1. Griffiths, David J. Introduction to Elementary Particles

2. "Quantum Diaries" [Internet]. [cited 2022 February 15]. Available from: https://www.quantumdiaries.org

3. Süngü YJ, Veli E. Exotic Hadrons. Marmara Fen Bilimleri Dergisi (2018) p:77-93

4. An, Liupan. "Experimental review of hidden-charm states" (2021)

5. "J/ψ particle" [Internet]. [cited 2022 February 15]. Available from: https://www.britannica.com

6. Xiao,T., et al. "Observation of the charged hadron $Z_c^{\mp}(3900)$ and evidence for the neutral $Z_c^0(3900)$ in $e^+e^- \rightarrow \pi\pi J/\psi$ and $\sqrt{s}$=4170 MeV." arXiv preprint:1304.3036 (2013)

7. Maiani, Luciano, et al. "Four quark interpretation of $Y(4260)$." Physical Review D 72.3 (2005):031502

8. "The PANDA experiment at FAIR in Darmstadt" [Internet]. [cited 2022 February 20]. Available from: https://panda.gsi.de

9. Kester, O., et al. "Status of the FAIR accelerator facility." Proceedings of IPAC2014, Dresden, Germany (2014):2084-2987

10. Krücken, Reiner and NUSTAR Collaboration. "The NUSTAR facility at FAIR." Journal of Physics G: Nuclear and Particle Physics 31.10 (2005): S1807

11. Jürgen, Eschke. "Compressed baryonic matter experiment at FAIR." EPJ Web of Conferences.Vol.20 EDP Sciences, 2012

12. Schwarz, Carsten and PANDA Collaboration " Journal of Physics: Conference Series.Vol.374 No.1. IOP Publishing, 2012

13. Stöhlker, Th, et al. "APPA at FAIR: From fundamental to applied research" Nuclear Instruments and Method in Physics Research Section B: Beam Interactions with Materials and Atoms 365 (2015): 680-685

14. Barucca G, et al. PANDA phase one. The European Physical Journal A, 57.6 (2021): 1-36.

15. "What does the term 'strangeness' refer to?" [Internet]. [cited 2022 March 30]. Available from: https://www.physlink.com

16. Panda Collaboration and James Rıtman. "The PANDA dedector at the GSI-FAIR project. " Internal Journal of Modern Physics A 20.02n03 (2005): 567-569

17. Belias, A. "FAIR status and the PANDA experiment" Journal of Instrumentation 15.10 (2020): C10001.

18. Schwarz, C, et al. "The Barrel DIRC of PANDA." Journal of Instrumentation 7.02 (2012): C02008.

19. Destafanis, Marco and PANDA Collaboration. “The PANDA experiiment at FAIR. “Nuclear Physics B-Proceedings Supplements 245 (2013): 199-206

20. Köseoglu, I, and PANDA Cherenkov Group. “Design of the Barrel and endcap DIRC dedectors for particle identification in PANDA.” International Journal of Modern Physics A 35.34n35 (2020): 2044020

21. Schwiening, J. “The Barrel DIRC dedector for the P^{-}ANDA experiment at FAIR.” Nuclear Instruments and Methods in Physics Research Section A:Accelerators, Spectrometers, Detectors and Associated Equipment 639.1 (2011): 315-318

22. Schwarz, C., et al. “The Barrel DIRC of PANDA.” Journal of Instrumentation 7.02(2012): C02008.

23. Kratochwil, N., et al. “Barrel Time-of-Flight (TOF) Dedector for the PANDA Experiment at FAIR.”

24. Abazov, Victor, et al. “Panda Muon System Prototype. “ EPJ Web of Conferences Vol.177. EDP Sciences, 2018

25. “Physics Requirements to The Muon System” [Internet]. [cited 2022 April 13]. Available from: https://panda.gsi.de

26. Smyrski, Jerzy and PANDA Collaboration. “Overview of The PANDA Experiment." Physics Procedia 37 (2012): 85-95.

27. “Range (muon) system for PANDA and SPD experiments” [Internet]. [cited 2022 April 23]. Available from: https://dlnp.jinr.ru

28. Groom, Donald E., Nikolai V. Mokhov, and Sergei l.Striganov. “Muon stopping power and range tables 10 MeV-100 TeV.” Atomic Data and Nuclear Data Tables 78.2 (2001): 183-356

29. Collaboration, P.A.N.D.A. “Technical Design Report for: PANDA Forward Time of Flight detector (FToF wall)” (2018).

30. Pflüger, Stefan. “Precise determination of the luminosity with the PANDA-luminosity detector and implementation of the helicity formalism for the ComPWA framework for an extraction of the scaler wave in the channel $J/\psi \rightarrow \pi^0\pi^0\gamma$ “ (2018).

31. Plazek, J, et al. “Track finding algorithm using the track road method for the PANDA Forward Tracker.” Journal of Computational Science 55 (2021): 101448

32. “Tracking System” [Internet]. [cited 2022 May 08]. Available from: https://panda.gsi.de

33. GEMs (Gas Electron Multiplier) – CMS Experiment [Internet]. [cited 2022 May 18]. Available from: https://cms.cern

34. A Gem of a detector [Internet]. [cited 2022 May 20]. Available from: https://cerncourier.com

35. Bouclier, Rager, et al. “The GAS Electron Multiiplier (GEM).” lEEE Transactions on Nuclear Science 44.3 (1997): 646-650

36. “Straw Tube Tracker” [Internet]. [cited 2022 May 29]. Available from: https://panda.gsi.de

37. Preston, Markus, et al. “A feature-extraction and pile-up reconstruction algorithm for the forward-spectrometer EMC of the PANDA experiment.” Nuclear Instruments and Methods in Physics Research Section A: Accelerators, Spectrometers, Detectors and Associated Equipment 1001 (2021):165501.

38. Sparato, Stefano and PANDA Collaboration. ”The PandaRoot framework for simulation,reconstruction and analysis.” Journal of Physics: Conference Series. Vol: 331. No:3. IOP Publishing, 2011.

39. Steinschaden, D, and PANDA Collaboration. “Event Reconstruction and Simulation in PandaRoot for the PANDA experiment.” Journal of Physics: Conference Series. Vol: 1085. No:4. IOP Publishing, 2018.

40. Spataro, Stefano. “Simulation and event reconstruction inside the PandaRoot framework.” Journal of Physics: Conference Series. Vol: 119 No:3. IOP Publishing, (2008

41. http://pdl.lbl.gov